J. Fluid Mech. (2014), *vol.* 756, *pp.* 384–421. © Cambridge University Press 2014
doi:10.1017/jfm.2014.405

Pressure fluctuations produced by forward steps immersed in a turbulent boundary layer

Manuj Awasthi[1], William J. Devenport[1,†], Stewart A. L. Glegg[2] and Jonathan B. Forest[1]

[1]Department of Aerospace and Ocean Engineering, Virginia Polytechnic Institute and State University, Blacksburg, VA 24061, USA

[2]Department of Ocean and Mechanical Engineering, Florida Atlantic University, Boca Raton, FL 33431, USA

(Received 29 September 2013; revised 10 July 2014; accepted 12 July 2014; first published online 2 September 2014)

Experiments have been performed on the disturbance of a high-Reynolds-number turbulent boundary layer by three forward steps with sizes close to 3.8, 15 and 60 % of the boundary layer thickness. Particular attention is focused on the impact of the steps on the fluctuating surface pressure field. Measurements were made from 5 boundary layer thicknesses upstream to 22 boundary layer thicknesses downstream of the step, a distance equivalent to over 600 step heights for the smallest step size. Flow speeds of 30 and 60 m s^{-1} were studied, corresponding to boundary layer momentum thickness Reynolds numbers of 15 500 and 26 600 and step size Reynolds numbers from 6640 to 213 000. The steps produce a disturbance to the boundary layer pressure spectrum that scales on step size and decays remarkably slowly with distance downstream. When normalized on step height and free-stream velocity, the disturbance is self-similar and appears to develop almost independently of the enveloping boundary layer. The disturbance is still clearly visible at 150 step heights downstream of the mid-size step. Pressure correlations show the disturbance to be characterized by organized quasiperiodic motions that become visible well downstream of reattachment. The coherence and scale of these motions, as seen in the wall pressure correlations, scales on the step height and thus their visibility relative to the boundary layer grows rapidly as the step size is increased.

Key words: boundary layer separation, boundary layer structure, turbulent flows

1. Introduction

The time-average topology of the incompressible turbulent flow over a forward facing step is well known. The flow is subject to an increasing adverse pressure gradient as it approaches the step that ultimately causes separation of the boundary layer, usually 1–2 step heights upstream. The flow then reattaches to the step face and is accelerated towards the salient edge of the step where it separates once more. This primary separation region closes when the flow reattaches, usually some 2–4 step heights downstream.

† Email address for correspondence: devenport@vt.edu

https://doi.org/10.1017/jfm.2014.405 Published online by Cambridge University Press

The step generates turbulence additional to that of the inflow boundary layer as part of the adverse pressure gradient flow upstream and in the shear layer and reattachment region of the primary separation. The turbulence, and the enhanced pressure fluctuations it produces, are generally thought to persist for a large distance downstream of the step. The persistence and decay of this pressure signature is important since it has a potential impact on the noise generated by downstream trailing edges or other geometrical elements, and serves as an important component of the forcing function for panel vibration if the flow surface is flexible. In most practical applications (such as the steps in a vehicle fuselage or hull) the step is likely to be a fraction of the boundary layer thickness, and can be as small as a few per cent.

The forward-facing step is part of a broader family of step configurations (including the backstep, square rib and blunt flat plate) that have attracted significant attention in the literature over the last 35 years. However, relatively few experimental studies have considered forward steps that are small compared with the oncoming boundary layer thickness, and none have looked in detail at the far-downstream pressure disturbance that forward steps produce. Perhaps the most relevant prior study here is due to Farabee & Casarella (1986) who examined flow over a forward step immersed in a boundary layer 2.4 times as high and with a momentum thickness Reynolds number $Re_\theta = 4079$, and step-height Reynolds number $Re_h = 21\,000$. They found that the step increased pressure fluctuations at low frequencies in the approach boundary layer and suppressed them at high frequencies. This effect was first visible about 6 step heights upstream ($x/h = -6$) and was seen to become quite large (of the order of 20 dB enhancement and suppression) at the step face. Farabee and Casarella found the streamwise coherence of pressure fluctuations upstream of the step to be reduced at low frequencies, a result they attributed to rapidly changing pressure statistics near the step and took to indicate that there was no single coherent source of pressure here. Immediately downstream of the step pressure fluctuations were seen to be greatly elevated across the spectrum but particularly at lower frequencies. Just aft of the step edge, Farabee & Casarella's (1986) surface pressure spectra show a maximum at the very low frequency of $fh/U_\infty \cong 0.03$, $fx_r/U_\infty \cong 0.1$, where x_r is the distance from the step to reattachment. Root-mean-square (r.m.s.) pressure fluctuation levels were observed to grow with distance downstream from the step with the maximum occurring in the vicinity of the reattachment point, near $x/h = 3$ where spectra had a peak at a frequency of $fh/U_\infty \cong 0.15$, $fx_r/U_\infty \cong 0.5$. Downstream of reattachment the flow remained highly energized with the decay back towards the undisturbed boundary layer levels proceeding most rapidly at high frequencies, and the peak frequency falling gradually with downstream distance. However, even at their last measurement station, 36 step heights downstream, Farabee and Casarella found that pressure fluctuations at low frequencies were still as much as 10 dB more intense, and significantly more coherent than in the approaching boundary layer.

The low-frequency fluctuations present in reattaching flows, such as those apparent in Farabee and Casarella's, may arise from the slow flapping of the separated shear layer and the quasiperiodic shedding of eddies from the downstream end of the separation bubble. These mechanisms, discussed by Eaton & Johnston (1981) and others in connection with backstep flows, have been observed and extensively catalogued by Kiya & Sasaki (1983, 1985) and Cherry, Hillier & Latour (1984) for blunt flat plates, arguably a close relative of the forward step configuration. The blunt flat plate flow is essentially a forward step flow, with a step height equal to half the plate thickness, but without an incident boundary layer and the upstream

https://doi.org/10.1017/jfm.2014.405 Published online by Cambridge University Press

separation that it produces. This difference results in a longer reattachment length, of about 10 step heights. This effect that can be attributed to the absence of inflow turbulence to the step corner, since adding free-stream turbulence to the blunt flat plate flow produces a large reduction in the length of the separation (Hillier & Cherry 1981). The studies of Kiya & Sasaki (1983, 1985) and Cherry *et al.* (1984) included flow visualizations and coordinated measurements of velocity and surface pressure fluctuations that showed the presence of two distinct mechanisms controlling the turbulence structure; the quasiperiodic shedding of eddies from the reattachment region, at a frequency $fx_r/U_\infty \cong 0.6$ ($fh/U_\infty \cong 0.06$), and the flapping or 'breathing' of the separation bubble shear layer, at a frequency $fx_r/U_\infty \cong 0.12$ ($fh/U_\infty \cong 0.012$). Pressure spectra measured very close to separation show evidence of the first mechanism, whereas those measured near reattachment indicate the presence of the second. Extensive study of a backstep flow (Lee & Sung 2002) using wavelet analysis of surface pressure fluctuations over the first 10 step heights downstream of the step revealed the shedding frequency to be $fh/U_\infty = 0.063$, or ($fx_r/U_\infty = 0.44$) in this case, quite similar to the blunt flat plate value.

The extent of the upstream influence of a forward step on the fluctuating pressure field has been studied Efimtsov *et al.* (1999). They studied steps whose size was between 1 and 20 % of the boundary layer thickness for boundary layers with displacement thickness Reynolds number from $3500 \leqslant Re_{\delta^*} \leqslant 428\,400$, including measurements in both the subsonic and supersonic regimes. They observe that while the pressure fluctuations due to step's presence can exceed those on a smooth wall by over 20 dB for larger steps, the enhancement in pressure fluctuation levels can be seen further upstream for smaller steps, relative to the step height. In fact, they state that in some cases the wall pressure spectrum can be influenced as far as 100 step heights upstream of the step. The results of these wind tunnel studies were extended to flight data in the experiments of Efimstov *et al.* (2002) and Steinwolf & Rizzi (2006).

Studies of the fluctuating pressure field generated by a forward step in the vicinity of the primary separation region have been performed by Leclercq *et al.* (2001), Largeau & Moriniere (2007), Fiorentini *et al.* (2007) and Camussi *et al.* (2008). Leclercq *et al.* considered the flow over a forward step followed by backstep located 10 step heights downstream. The inflow boundary layer thickness was some 70 % of the step height and the step height Reynolds number 170 000. They performed laser Doppler anemometer (LDA) measurements of the mean and turbulent field as well as wall pressure fluctuation measurements using pairs of microphones. They found the shear layer separating of the forward facing step to be the most intense turbulence producer in the entire flow, with turbulence intensities reaching 40 % over the first half of the separation bubble. Wall pressure spectra measured from $x/h = 2$ to 9, under the bubble and in the reattachment region, show pressure fluctuations to be most intense at non-dimensional frequencies $fh/U_\infty \cong 0.16$, $fx_r/U_\infty \cong 0.5$ and to decay slowly with downstream distance. Above this frequency the spectra were seen to have an almost linear roll off (on a log–log scale) with a slope of -2 to -2.5. The streamwise coherence of pressure fluctuations was also found to be strongest at this frequency.

Largeau & Moriniere (2007) performed flow visualizations, particle image velocimetry (PIV) and coordinated surface pressure fluctuation and turbulence measurements over the first 8 step heights downstream of several forward facing steps exposed to an inflow turbulent boundary layer between 16 and 26 % of their height. The step-height Reynolds numbers varied between 12 800 and 28 800. They found that

https://doi.org/10.1017/jfm.2014.405 Published online by Cambridge University Press

the primary separation produced intense turbulence that influenced the wall pressure fluctuations, resulting in maximum r.m.s. pressures being reached near reattachment. They used pressure auto- and cross-correlations and velocity–pressure correlations to establish the frequency scale of the dominant motions, which they estimated at around $fh/U_\infty = 0.5$, $fx_r/U_\infty \cong 1.8$ in the separation region and 20 % higher after reattachment. They discuss this in the context of the flapping and shedding mechanisms discussed above, although these frequencies are considerably higher than those seen in other studies.

Fiorentini *et al.* (2007) and Camussi *et al.* (2008) examined the fluctuating wall pressure field and mean velocity field in the vicinity ($-6 < x/h < 8$) of a step in a large water channel for $Re_h = 4400$–$26\,300$. Their measurements also included correlations between wall pressures and time-resolved PIV images of the velocity field. The step height was twice the incoming boundary layer displacement thickness and therefore, presumably, about a quarter of the incoming boundary layer height. They found that the distance to reattachment in the primary separation region increased quite strongly with Reynolds number (from $1.5h$ to $2.1h$ for $Re_h = 8800$–$26\,300$), and that pressure spectra measured under the separation bubble and reattachment regions decayed slowly with downstream distance and were characterized by a power law roll-off with a slope of -2 to -2.5, consistent with Leclercq *et al.* (2001). Pressure spectra downstream of the step showed the greatest increase in energy at $fh/U_\infty \cong 0.2$, $fx_r/U_\infty \cong 0.4$, and pressure velocity correlations showed a dominant time scale consistent with this. Convection velocities of the pressure disturbance increased from about $0.4U_\infty$ in the separation bubble at $x/h = 1$ to about $0.66U_\infty$ downstream of reattachment near $x/h = 6$. Camussi *et al.* (2008) also made a number of observations on the flow just upstream of the step. Like Farabee & Casarella (1986), they observed the rapid increase in low-frequency pressure fluctuations as the step is approached accompanied by a reduction at high frequencies. They attribute this to the flapping of the shear layer of the upstream separation region at very low frequencies $fh/U_\infty \cong 0.01$.

There appear to be no studies of the surface pressure disturbance produced by a forward step that go beyond 36 step heights examined by Farabee & Casarella (1986). However, there have been studies of the turbulent velocity field. Tachie, Balachandar & Bergstrom (2001) also studied a small step ($h/\delta \cong 8\,\%$) immersed in low-Reynolds-number turbulent boundary layers ($1010 \leqslant Re_\theta \leqslant 1890$) produced in a water channel. They studied the mean velocity and turbulence intensity profiles at $x/h = 1$, 10, 20, 50, 100 and 162 and found that the mean velocity profiles recovered to their undisturbed step heights by about $x/h = 50$. By $x/h = 100$ the turbulence profiles still had not recovered their undisturbed form, but instead had developed a new self-similar shape: a possible indication of a very long lived disturbance. Boundary layer development downstream of reattachment for a blunt flat plate was studied by Castro & Epik (1998). They studied turbulent mean velocity, velocity fluctuations, shear stress and other turbulence quantities. They found that turbulence structure had not recovered to equilibrium conditions even after 20 reattachment lengths downstream of the leading edge (equivalent to some 60 step heights for a forward step). They attributed this to the presence of large energized structures which exist around reattachment position and which can only slowly recover to equilibrium conditions.

In addition to experiments, recent large eddy simulations by Ji & Wang (2010, 2012) have also provided new physical insight into the behaviour of the forward step flow, in particular the nature of the wall pressure fluctuations as well as the role of the

https://doi.org/10.1017/jfm.2014.405 Published online by Cambridge University Press

turbulence in generating sound. They performed four forward step-flow calculations with step heights equivalent to 0.83, 3.3, 13 and 53 % of the approach boundary layer thickness. Step height Reynolds numbers ranged from 328 to 21 000 and the inflow boundary layer had a Reynolds number Re_θ of 4755. The largest of these step cases was designed to match the experiment of Farabee & Casarella (1986) and for this case the calculations show quite good agreement with the experimental results. The r.m.s. wall pressure fluctuations, including the maximum in the reattachment region are accurately predicted, and wall pressure spectra agree with experimental results up to a frequency $fh/U_\infty \cong 0.5$ beyond which computed levels are attenuated by the finite grid resolution of the simulation. Ji & Wang (2010) observe evidence in the pressure spectra of the shedding of eddies from the largest forward step at a frequency of $fh/U_\infty \cong 0.2$, $fx_r/U_\infty \cong 0.6$, in agreement with experimental studies. They observe that pressure spectra predicted in the reattachment region can be scaled using the reattachment length, and show a roll-off with frequency that follows a $-7/3$ slope, on a log–log scale, also consistent with experimental efforts cited above. They argue that the early development of the shear layer shed from the step edge is the primary sound source in this flow, because of its proximity to the step corner and the focusing of the Green's function here. Particularly interesting are the changes to the flow predicted with change in the step size. The size of the primary separation bubble falls rapidly as the step size (and Reynolds number) is reduced and disappears altogether for the 3.3 and 0.83 % step heights. At the same time the separation region upstream of the step was seen to flatten with the separation point moving upstream from the step. Also as the step size is reduced, the peak in the r.m.s. pressure fluctuations reduces and, as the primary separation bubble disappears, moves upstream of the step. They found that p_{rms} could not be consistently scaled on any one component of the Reynolds stress tensor of the overriding flow. The decay of p_{rms} downstream of the steps was examined for the two larger steps where the flow separated from the step. Ji and Wang observed that 60 % of the peak p_{rms} had dissipated within three reattachment lengths of the step, but the subsequent recovery is much slower. Extrapolating their calculations downstream they argue that recovery of the pressure fluctuations to their undisturbed form could take almost 300 step heights.

The focus of the present study is the pressure fluctuation disturbance produced by small steps immersed in turbulent boundary layers at high Reynolds number. In particular, we are interested in the form and the decay of the disturbance over large distances downstream of reattachment, which has largely been neglected in the literature. This paper describes an experiment to examine the disturbance due to three steps equal in height to 3.8, 15 and 60 % of the incoming boundary layer thickness, deliberately matching at higher Reynolds number three of Ji & Wang's (2010, 2012) configurations. This experiment also provides a useful comparison with Farabee & Casarella's (1986) study. Particular attention is focused on the impact of the steps on the spectra and correlations of the fluctuating surface pressure field upstream and far downstream of the step (over 600 step heights for the smallest step). The configurations studied had inflow boundary layer momentum thickness Reynolds numbers of 15 500 and 26 600 and step size Reynolds numbers from 6640 to 213 000. Our major conclusion is that the pressure disturbance becomes self-similar downstream of the reattachment region ($x/h > 8$) with a form almost independent of streamwise position, step size and Reynolds number. The disturbance is associated with an organized quasiperiodic structure that scales on the step height and appears to evolve independently of the boundary layer within which it is immersed.

https://doi.org/10.1017/jfm.2014.405 Published online by Cambridge University Press

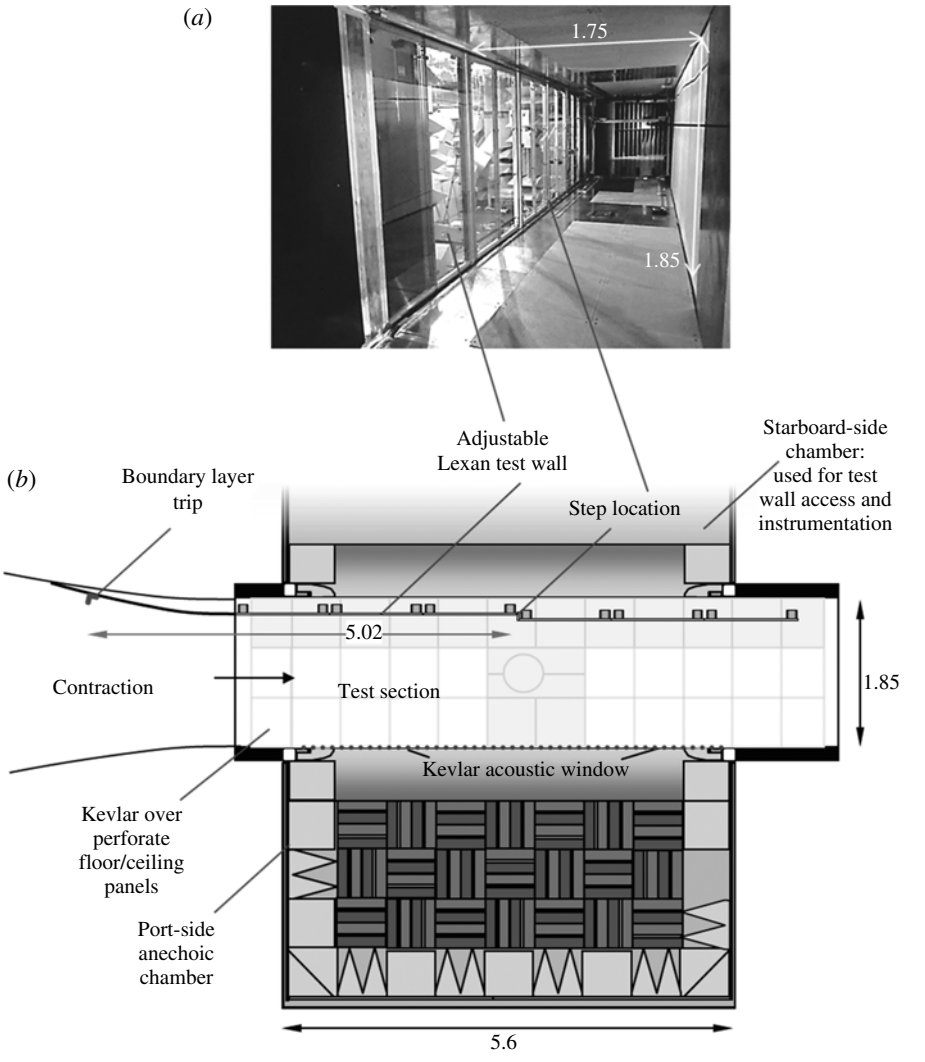


FIGURE 1. The anechoic test section system and test wall. (a) Photograph showing the test section and test wall as seen from upstream. (b) Plan view schematic showing the test section, test wall and anechoic chambers. Dimensions in metres.

2. Experimental set-up

2.1. *Wind tunnel and step configurations*

Measurements were performed in the Stability Wind Tunnel at Virginia Tech (figure 1). The wind tunnel is unusual in that it can be run in both aerodynamic and anechoic configurations. The anechoic test section, which is sandwiched between two anechoic chambers, was used here (Devenport *et al.* 2013). The test section is 7.3 m long and has a square cross-section measuring 1.85 m on edge. Flow through the empty test section is closely uniform and has a turbulence intensity of 0.024 % at 30 m s^{-1} and 0.031 % at 57 m s^{-1}. Top speed in the test section is some 80 m s^{-1}.

The acoustically absorbent floor and ceiling of the test section consist of Kevlar-covered metal perforate panels backed by acoustic wedges. In its normal

https://doi.org/10.1017/jfm.2014.405 Published online by Cambridge University Press

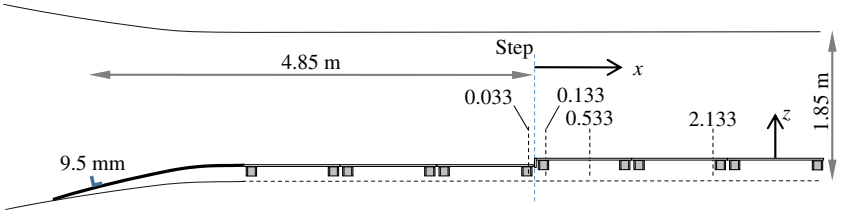


FIGURE 2. (Colour online) Geometry of the test wall showing coordinate system principal measurement stations. Coordinate y is measured spanwise from the centreline of the test wall, and is into the plane of the paper in this figure.

configuration both sidewalls are formed from large tensioned panels of Kevlar cloth. These contain the flow and eliminate the need for a jet catcher while allowing sound generated in the flow to pass into the anechoic chambers on either side. While sound measurements were not made in the present study, this setup provided an acoustically quiet configuration well suited to surface pressure measurements. For the present work, one of the Kevlar side-wall panels was removed, and an adjustable test wall suitable for growing high-Reynolds-number two-dimensional turbulent boundary layers was installed (figure 1). The wall covered the full 1.85 m height of the test section and extended upstream into the contraction where a curved section was used to fair this surface to the tunnel sidewall. The curved section of wall had a streamwise extent of 2.44 m upstream of the test section entrance. The remainder of the false wall extended 7.32 m downstream of the test section entrance, providing a total of 9.76 m for boundary layer growth and development.

The main part of the test wall was fabricated from a series of six reinforced Lexan panels. The panel mounting mechanism enabled adjustment of the panel positions so as to produce a zero-pressure-gradient flow or so that step configurations could be produced. Forward steps were made by moving the last three test section panels while keeping those upstream in their zero-pressure-gradient configuration (see figure 2). This placed the step location 3.66 and 4.85 m downstream of the test section entrance and boundary layer trip location, respectively. The 9.5 mm high trip consisted of a simple two-dimensional fence, created using a strip of aluminum angle mounted with its flange on the downstream side. The perpendicular face of the step was fabricated from 12.7 mm thick machined Lexan sheet, with care being taken to ensure that the salient edge remained clean and sharp along its 1.8 m span. The Lexan panels were instrumented with 0.5 mm diameter pressure taps (in spanwise and streamwise arrays) and with attachments for surface-penetrating instrumentation, including microphones and hotwire probes to be introduced and operated from the unused anechoic chamber on the outside of the test wall.

In total, four wall configurations were studied. In the ‘smooth-wall’ configuration, with no step, the wall was adjusted merely to minimize any streamwise and spanwise pressure gradients. Measurements made in this configuration served as the control for judging the disturbances created by the steps. Three forward step configurations with step sizes h of 3.65, 14.6 and 58.4 mm were also generated. Note that the medium and large step sizes are, respectively, 4 and 16 times that of the smallest. A high aspect ratio is essential to maintaining two-dimensionality in step flows. The aspect ratio (span to height) of the present steps was 500, 125 and 31.3 respectively, far exceeding the normal requirement of 10–15 (e.g. Cherry *et al.* 1984).

https://doi.org/10.1017/jfm.2014.405 Published online by Cambridge University Press

The coordinate system used in this paper is centred at the mid-span of the step location (see figure 2). Distance x is measured in the downstream direction, y spanwise and z perpendicular to the test wall. The origin for z is the surface of the test wall itself, and so this origin is different upstream and downstream of the steps. Velocity components u, v and w are defined in the x, y and z directions, respectively.

2.2. *Instrumentation*

Free-stream velocity was monitored using a Pitot static probe located at $(x, y, z) = (-0.44\text{ m}, -0.59\text{ m}, 1.25\text{ m})$. Free-stream dynamic pressure was monitored using either a Datametrics Barocel Pressure Sensor Type 590D, or the Esterline NetScanner Model 98RK pressure scanner also used to measure the mean pressure at the static taps. Temperature in the test section was monitored using an Omega Thermistor type 44004 (accuracy $\pm 0.2\,^{\circ}\text{C}$) and the ambient absolute pressure was determined using a Validyne DB-99 Digital Barometer (resolution 0.01″ Hg).

2.2.1. *Measurement of wall pressure fluctuations*

Wall pressure fluctuations were measured using B&K 4138, 1/8th inch pressure-field microphones. These microphones provide a high degree of spatial resolution due to their small size and thus provide useful data that can be used for correlating pressure fluctuation at small distances. Moreover, due to their high dynamic range (52.2–168 dB) they are suitable for higher flow speed measurements where the magnitude of pressure fluctuations can be significant. To improve spatial resolution further these microphones were operated with the salt-and-pepper shaker caps removed and replaced with caps containing 1/2 mm diameter pinholes, custom manufactured by B&K. Previous measurements under a wall jet boundary layer, by Devenport *et al.* (2011) showed a 1/2 mm pinhole to be sufficiently small to resolve pressure fluctuations up to 20 kHz.

Before and after testing, the amplitude and phase response of the microphone/pinhole combinations were calibrated in an acoustic chamber using a white noise source against an unaltered model 4138 microphone which was used as a reference. The white noise source was created by an Agilent VXI data acquisition system and a University Sound ID60C8 speaker. The amplitude gain of the microphones was calibrated daily using a B&K type 4228 Pistonphone operating at 250 Hz. The pinhole caps resulted in the microphones having a resonant peak in their response at around 15 kHz. A typical calibration is shown in figure 3. Subsequent to the test, the shape of this peak was found to be a weak function of the speed of the tunnel flow. Fitting the calibrations to a second-order system model, it was found that damping decreased as the flow speed increased and there was a slight reduction in the resonant frequency. These effects were accounted for in the final data reduction, allowing calibrated surface pressure fluctuations to be obtained up to 20 kHz.

A total of seven microphones were used for the measurements. For all measurements the microphone outputs were sampled simultaneously using two 24-bit B&K 3050-A LXI modules sampling at 65 536 Hz for 32 s. The microphones were placed at many different configurations for each of the four smooth wall/step flows. Five of the microphones were grouped into a 132 mm long linear array. The microphones in the array were unevenly spaced so as to define 10 distinct separations from 6.5 to 132 mm. For some of the cases, an additional single microphone was placed relative to the array to define an additional five separations. For all measurements a reference microphone (without pinhole) was used to monitor and cancel any

https://doi.org/10.1017/jfm.2014.405 Published online by Cambridge University Press

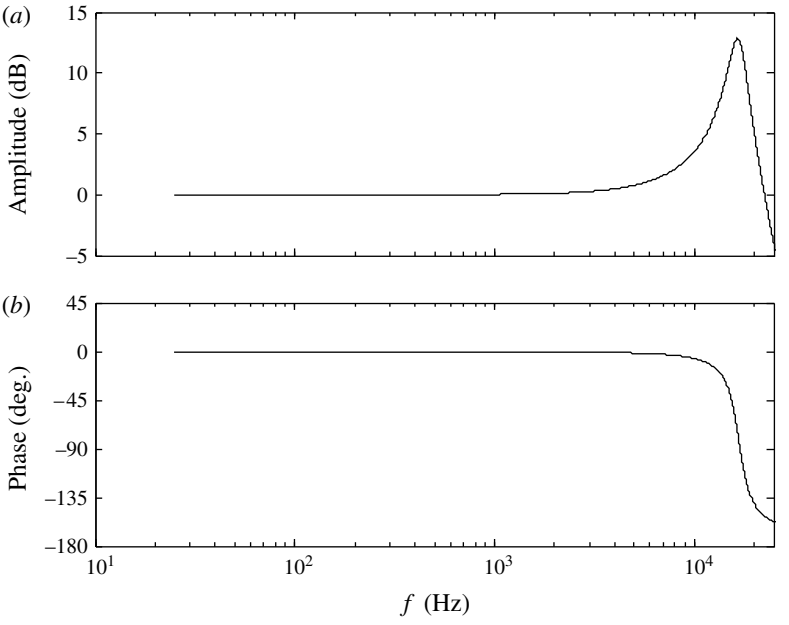


FIGURE 3. Dynamic response calibration of one of the B&K 4138, 1/8″ pressure-field microphones with 1/2 mm pinhole: (*a*) amplitude; (*b*) phase.

acoustic contamination of the six measurement microphone signals. A typical set of measurement locations for one of the flow configurations is shown in figure 4. This particular distribution, which was measured with the 14.6 mm step, involves 30 different microphone arrangements. For each of the arrangements, the five-microphone array was placed spanwise at one of four streamwise locations: $x = -0.033$, 0.133, 0.533 and 2.133 m, or was placed streamwise in one of four positions straddling these locations, as shown. The single microphone was placed at various locations for each of these arrangements, when used. Due to failure of one of the microphones, arrangements used for the smooth wall and largest step did not include the single microphone. Note that the three principal downstream measurement stations of $x = 0.133$, 0.533 and 2.133 m, differ by factors of four. With the same factor separating the step sizes, this distribution allows comparison of the results measured at the same x/δ and x/h positions.

For each arrangement, the reference microphone was placed at $y = -358$ mm and at an x location close to the streamwise position of the array or the single microphone, whichever was the focus of the measurement. At this position there was no significant correlation between turbulent pressure fluctuations sensed by the reference and measurement microphones. Any correlation was therefore assumed to be a measurement of the parasitic tunnel noise and removed from the measurement microphone spectra. The removal was performed by applying the method of Horne (1990), as follows. Consider the pressure fluctuation sensed at two locations of interest p_1 and p_2. Both signals are composed of the desired turbulent boundary layer component (p_{1_t}, p_{2_t}) and a parasitic acoustic noise contribution uncorrelated with the boundary layer component (p_{1_a}, p_{2_a}). The scheme allows for all of these contributions to be different. Next consider the pressure fluctuation measured at a reference location p_r experiencing an uncorrelated turbulent pressure fluctuation (p_{r_t})

https://doi.org/10.1017/jfm.2014.405 Published online by Cambridge University Press

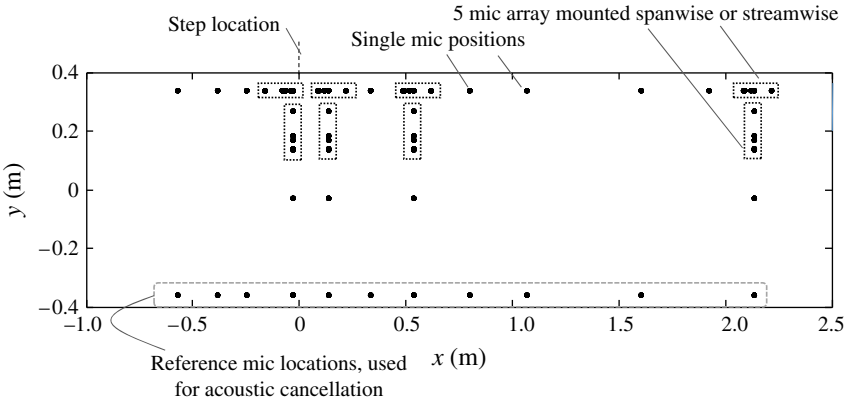


FIGURE 4. Microphone measurement locations (●). Dotted rectangles indicate locations associated with placement of the five-microphone array. Other locations correspond to single microphone placements. The grey dashed rectangle encloses locations at which the reference microphone, used for acoustic cancellation, was positioned.

but the same contaminating acoustic signal p_{1_a}. The uncontaminated cross-correlation or cross-spectrum between p_1 and p_2 simply as the cross-spectrum between $(p_1 - p_r)$ and p_2, since $p_1 - p_r$ contains no parasitic contribution, and there is no correlation between p_{2_t} and p_{r_t}. The same method with $p_1 = p_2$ is used to remove contamination from autospectra and autocorrelation data.

Acoustic contributions, believed to originate predominantly from the wind tunnel fan, were only found to be significant at frequencies less than 20 and 40 Hz for flow speeds of 30 and 60 m s^{-1}, respectively. Acoustic wavelengths at these low frequencies are very large (>8.5 m) compared with the test section width of 1.83 m and the contamination would thus have been in-phase across the test section, consistent with the cancellation scheme. It is possible that this method resulted in subtraction of some acoustic pressure fluctuations generated by the boundary layer itself, but only at acoustic wavelengths that would have been heavily influenced by their confinement in the test section.

2.2.2. *Hot-wire anemometry*

Auspex Corporation model AVOP-4-100 four-sensor hot-wire probes were used to obtain three-component mean velocity and turbulence measurements in the undisturbed boundary layer. Probes were mounted on a tunnel traverse system capable of movement in all three dimensions. Four Dantec Dynamics 90C10 StreamLine Constant Temperature Anemometers were used to operate the sensors. Hot-wire signals were recorded using a 64-channel 16-bit Agilent E1432 digitizer and signal analyser. Flow temperature was monitored continuously during hot-wire measurements and corrections made using the method of Bearman (1971).

Probes were calibrated directly for a three-dimensional flow angle using the look-up table method of Wittmer, Devenport & Zsoldos (1998) and for velocity based on King's law. Angle calibrations, which depend primarily on sensor geometry were performed in the potential core of a jet before and after the experiment. Frequent velocity calibrations were performed during the experiment in the wind tunnel free stream. The AVOP-4-100 has a 1 mm^3 measurement volume and can be used up to

https://doi.org/10.1017/jfm.2014.405 Published online by Cambridge University Press

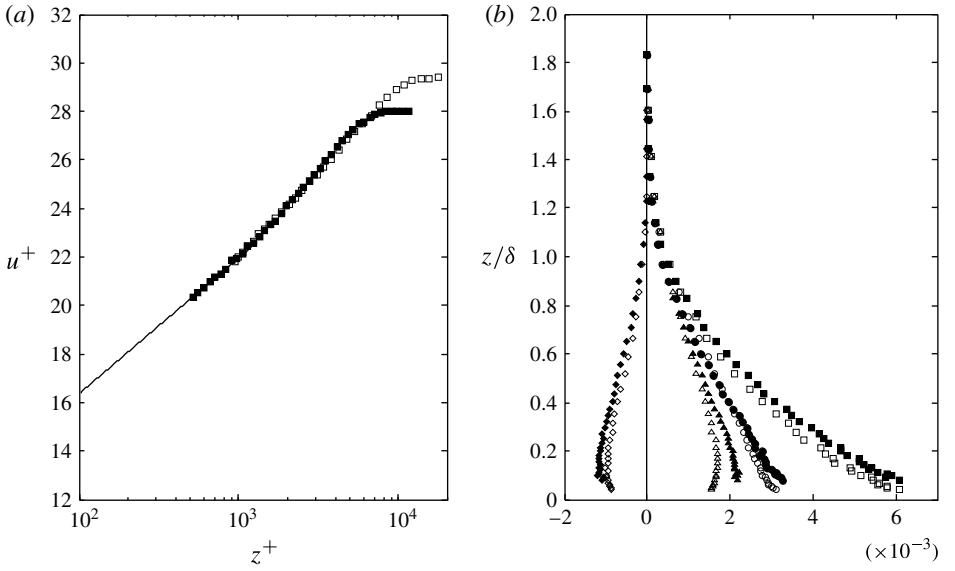


FIGURE 5. Boundary layer profiles measured at $x = -152$ mm with the four-sensor probe and without the step for 30 m s^{-1} (filled symbols) and 55 m s^{-1} (open symbols). (*a*) Mean streamwise velocity, solid line is $u^+ = (1/0.41)\ln(y^+) + 5.1$, (*b*) turbulence stresses; □, $\overline{u'^2}/U_\infty^2$; ○, $\overline{v'^2}/U_\infty^2$; △, $\overline{w'^2}/U_\infty^2$; ◇, $\overline{u'w'}/U_\infty^2$.

approximately 3 mm from a wall before velocity gradient errors become significant (see Wittmer *et al.* 1998).

3. Results and discussion

3.1. *Inflow boundary layer and wall pressure statistics*

Hotwire velocity and turbulence measurements of the zero-pressure-gradient turbulent boundary layer produced with no step were made at $x = -152$ mm in order to determine the form and parameters of the boundary layer in the absence of the step. Spanwise and cross-sectional measurements were also made at this station in order to verify the two-dimensionality of the flow.

While all other measurements made in this study were performed at free-stream velocities of 30 and 60 m s^{-1}, hotwire measurements were made at 30 and 55 m s^{-1} due to vibration problems with the probe traverse at the higher speed. Mean-velocity and turbulence-stress profiles measured at the centre span of the wall are shown in figure 5. These show very similar flow structure at the two speeds, with the exception of a slight reduction (relative to U_∞) in turbulence levels as the flow speed is increased.

Table 1 shows flow conditions at 30 and 60 m s^{-1} at which all of the remaining measurements were made. Boundary layer, displacement and momentum thicknesses values (δ, δ^* and θ) at 60 m s^{-1} were assumed to be the same as those measured at 55 m s^{-1}. Note that boundary layer thickness was defined as the point where the turbulence intensity passed through 2 %, this being almost equivalent to the point of 99 %U_e but rather less uncertain. The law of the wall was used to complete the profiles between the lowest measured point and the flow surface for the integration of δ^* and θ. The three steps of height 3.65, 14.6 and 58.3 mm have step height to

https://doi.org/10.1017/jfm.2014.405 Published online by Cambridge University Press

	U_∞ (m s^{-1})	δ (mm)	θ (mm)	δ^* (mm)	Re_δ	Re_θ	h (mm)	h/δ (%)	Re_h
Present experiment	30	97	8.5	10.8	177 000	15 500	3.65	3.8	6 640
							14.6	15.1	26 600
							58.3	60.1	106 000
	60	95	7.3	8.8	346 000	26 600	3.65	3.8	13 300
							14.6	15.4	53 200
							58.4	61.5	213 000
Farabee & Casarella (1986)	25	30.5				4 079	12.7	41.7	21 000
Ji & Wang (2010, 2012)						4 755		3.3	1 620
								13.3	6 480
								53.3	25 920

TABLE 1. Boundary layer and step parameters for the pressure fluctuation measurements.

U_∞ (m s^{-1})	h (mm)	h/δ (%)	x_s/h	$\Delta x_s/h$	x_r/h	$\Delta x_r/h$
30	3.65	3.8	−1.9	0.4	2.3	1.4
	14.6	15.1	−1.9	0.4	3.6	0.6
	58.3	60.1			4.1	0.4
60	3.65	3.8	−1.5	0.7		
	14.6	15.4	−1.7	0.4	3.7	1
	58.4	61.5	−1.5	0.9	4.2	0.4

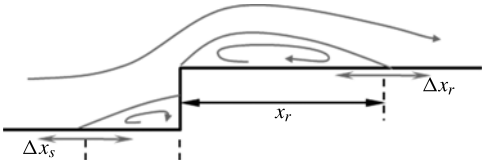


TABLE 2. Separation and reattachment locations.

boundary layer thickness ratios h/δ that vary from 3.8 up to 61.5 % and step height Reynolds numbers Re_h that vary from 6640 for the small step at 30 m s^{-1} to 213 000 for the large step at 60 m s^{-1}.

Table 1 also includes parameters and conditions for the experiments of Farabee & Casarella (1986) and the computations of Ji & Wang (2010, 2012), which are used as comparisons for the present experiments. Farabee and Cassarella studied a forward step flow with $h/\delta = 41$ % (most closely matching the present large step configuration) and $Re_h = 21\,000$ (nearest to the medium step at 30 m s^{-1}). Ji and Wang performed calculations for three forward steps with $h/\delta = 3.3$, 13.3 and 53.3 %, conditions the present experiment was designed to match. Step height Reynolds numbers were, however, four or eight times smaller than in the present study.

Table 2 lists forward separation and rearward reattachment locations x_s and x_r for the six step flows, determined using surface oil flow visualization (see the figure inset in table 2 for the definition of these positions). Such visualizations reveal the general region of separation or reattachment, the centre of which was used to determine x_s and x_r. The width of these regions Δx_s and Δx_r are also listed and these numbers can be interpreted as an indication of uncertainty and perhaps a measure

https://doi.org/10.1017/jfm.2014.405 Published online by Cambridge University Press

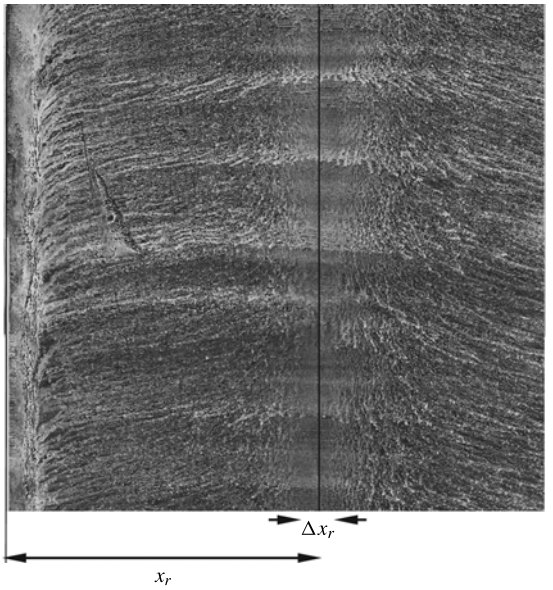


FIGURE 6. Sample oil-flow visualization showing the reattachment surface downstream of the 58.3 mm high step at 30 m s^{-1}. Flow is from left to right and the left-hand edge of the image represents the step corner. The action of gravity on this vertically oriented surface is visible in the general downward drift of the pigment streaks.

of extent of the separation or reattachment process. An example flow visualization is shown in figure 6. The upstream flow visualization was unreadable for the largest step at 30 m s^{-1} as was the downstream visualization for the smallest step at 60 m s^{-1}, hence the missing values. In all but one of the useable cases, the oil flow visualizations suggested reattachment approximately 4 step heights downstream of the step. The exception here is the small step at 30 m s^{-1} which showed reattachment at 2.3 step heights.

Farabee & Casarella (1986) estimated the reattachment length in their experiment to be 3–4 step heights, roughly consistent with the present results. Ji & Wang (2012) give reattachment at 2.93 step heights downstream and separation at 0.85 step heights upstream of their largest step. These numbers shrink and grow, respectively, as the step size is reduced and for their small step $h/\delta = 3.3\,\%$, they show no separation bubble on top of the step at all. Even accounting for uncertainties, Ji & Wang's (2012) calculations show shorter reattachment lengths than the present measurements. This is shown further in figure 7 which compares the present and Ji & Wang's (2012) values of x_r/h plotted as functions of h/δ and of Re_h. The data are scattered and show no clear dependence versus h/δ but collapse quite well to a single increasing curve when plotted against Re_h. Thus, the boundary layer thickness appears to be a secondary parameter in controlling the overall flow geometry. Furthermore, it appears that Ji and Wang's reattachment lengths are shorter because their Reynolds numbers were smaller by a factor of 4 or 8. These conclusions are partially consistent with the observations of Sherry *et al.* (2009) who argue that the reattachment length is a strong function of Reynolds number, but only weakly dependent on h/δ, for $h/\delta < 1$. However, they also argue that the reattachment length plateaus at step Reynolds numbers above 8500, which does not appear to happen in the present experiments.

https://doi.org/10.1017/jfm.2014.405 Published online by Cambridge University Press

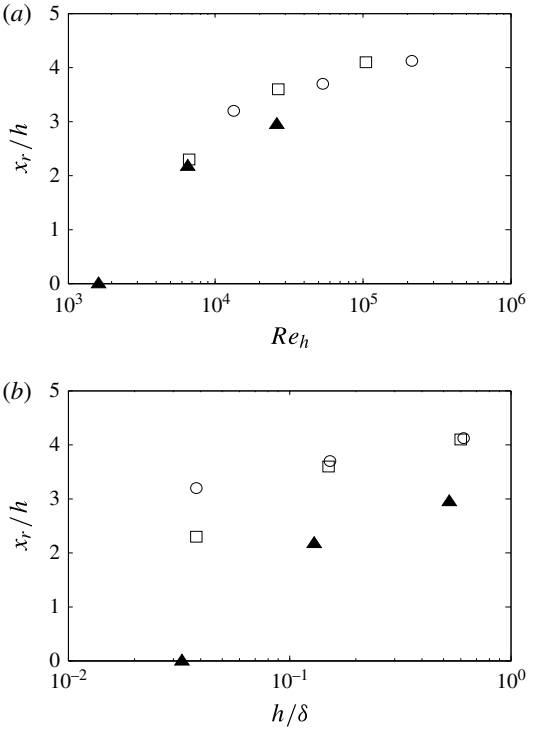


FIGURE 7. Comparison of reattachment lengths from the present experiment and from the calculations of Ji & Wang (2012) shown as functions of (*a*) step height Reynolds number and (*b*) step height to boundary layer thickness ratio. Note that reattachment length for the smallest step at 60 m s^{-1} in the present experiment was estimated from wall pressure measurements. □, present experiment 30 m s^{-1}; ○, present experiment 60 m s^{-1}; ▲, Ji & Wang (2010, 2012).

Distributions of mean pressure coefficient C_p measured on the test wall at $U_\infty = 30$ and 60 m s^{-1} are shown in figure 8. Figure 8(*b*) shows the spanwise pressure variation across the test wall at $x = 0.021$ m for each of the four configurations. These results, and similar measurements made at $x = 0.328$ m, show little spanwise variation confirming the near-two-dimensionality of these flows. Figure 8(*a*) shows the pressure distribution along the wall for all four configurations in the vicinity of the step. Regardless of step size, the pressure rises from the free-stream value as the step is approached to a maximum at its forward face. The pressure immediately downstream of the step is much lower than in the free stream as a result of the acceleration of the flow over the salient edge of the step and its separation there. Pressure then rises as a consequence of the reattachment of the separated shear layer, eventually recovering to a constant value. For the small and medium step at both speeds, this constant value is indistinguishable from the free-stream pressure. This is a consequence of the large size of the test section and thus the almost negligible effect of the contraction of the flow produced by the small and medium steps. For the large step, the mean pressure coefficient remains slightly negative at -0.06 following the recovery from reattachment. This is consistent with the overall 3.3 % contraction produced by the step in this case. This is not a large effect, however, and in all cases the present setup provides a close approximation of unbounded external flow over a step.

https://doi.org/10.1017/jfm.2014.405 Published online by Cambridge University Press

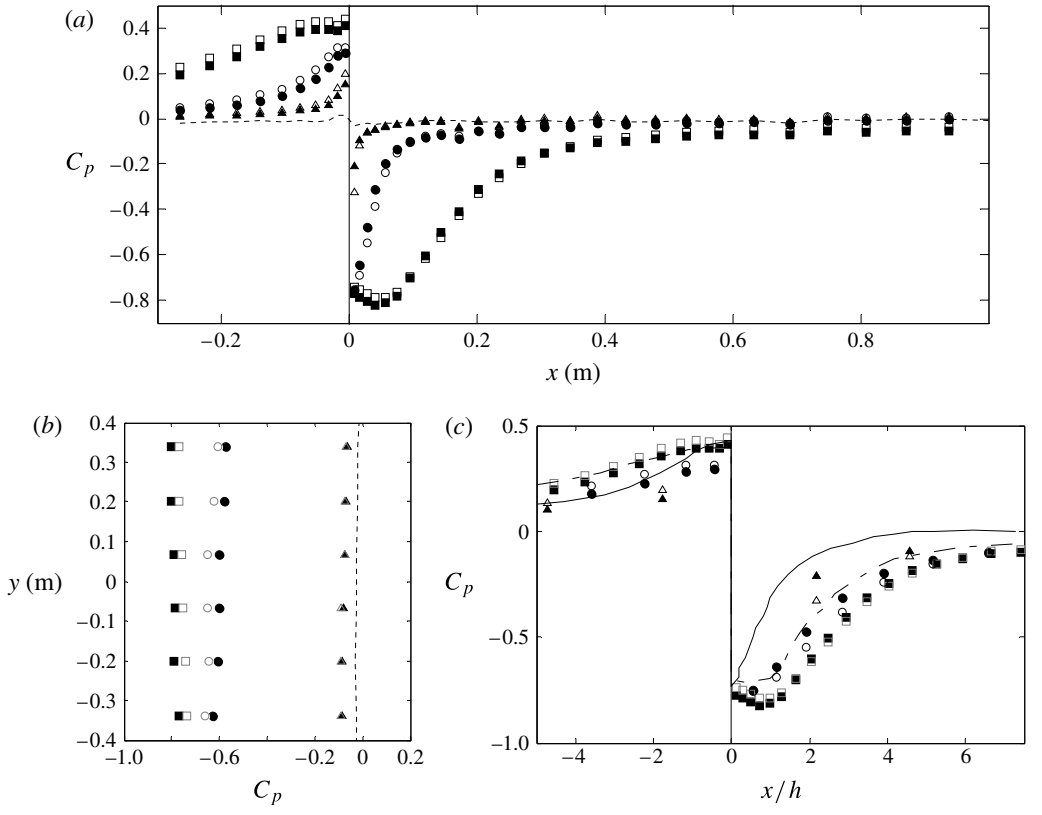


FIGURE 8. Mean pressure coefficient measured on the test wall for the four configurations (*a*) as a function of streamwise position, (*b*) as a function of spanwise position at $x = 0.021$ m, (*c*) as a function of streamwise position normalized on step height. ■, $h = 58.4$ mm, 30 m s^{-1}; ●, 14.6 mm, 30 m s^{-1}; ▲, 3.7 mm, 30 m s^{-1}; □, 58.4 mm, 60 m s^{-1}; ○, 14.6 mm, 60 m s^{-1}; △, 3.7 mm, 60 m s^{-1}; ----, smooth wall; —, Farabee & Casarella (1986); – – –, Ji & Wang (2010, 2012) $h/\delta = 53.3\,\%$.

Figure 8(*c*) shows these same step pressure distributions plotted against x/h. In this view we see clearly that the total pressure rise upstream of the step increases as the step size is increased. This occurs because a larger step penetrates further into the boundary layer and therefore produces the stagnation of higher momentum fluid on its forward face. There is a noticeable increase of approximately 0.05 in the magnitude of the pressure rise with a doubling of the Reynolds number for all three steps. On the downstream side we see that the pressure rise associated with reattachment moves gradually upstream as the step size is reduced. At the reattachment position for the large step at 30 m s^{-1}, $x/h = 4.1$, the pressure coefficient has recovered to -0.23. Assuming the same pressure recovery to reattachment in the medium step case at this Reynolds number implies reattachment at 3.6 step heights, in close agreement with the oil-flow visualizations. The same assumption applied to the 30 m s^{-1} small step case yields a reattachment length of 2.0 step heights. Applying the same scheme to the 60 m s^{-1} data we get reattachment lengths of 4.2, 4.1 and 3.2 step heights for the large, medium and small steps, respectively. Overall these numbers correlate quite well with the oil flow visualization results of table 2. Together these results indicate

https://doi.org/10.1017/jfm.2014.405 Published online by Cambridge University Press

an increase in reattachment length with Reynolds number that is particularly strong for the smallest step size, consistent with figure 7.

Figure 8(*c*) also includes pressure coefficient results from Farabee and Cassarella's measurements and from Ji and Wang's large step ($h/\delta = 53.3\,\%$). Despite representing nearly identical conditions, these two sources show substantial disagreement over the form of the mean pressure distribution, the pressure rises upstream and downstream of the step being more gradual in the calculation. The present measurements for the large step agree most closely with Ji and Wang's results. Interestingly, Ji and Wang's results, with a step Reynolds number Re_h of 25 920 match most nearly the present results for the medium step at 30 m s^{-1} ($h/\delta = 15.1\,\%$), with $Re_h = 26\,600$. This again suggests that Reynolds number may be a more important factor than step height to boundary layer thickness ratio in determining the overall form of the separation region.

Note that, in addition to the undisturbed boundary layer velocity measurements described above, turbulence and mean velocity profiles were measured both upstream and up to 148 step heights downstream of the 14.6 mm step at 30 m s^{-1}. Also, detailed two-point measurements were made of the spanwise and normal-to-wall space–time correlations in the undisturbed boundary layer and in the flow downstream of this step. These results are presented and discussed by Awasthi (2012).

3.2. *Wall pressure fluctuations*

3.2.1. *Root-mean-square pressure*

Root-mean-square pressure coefficient C_p', normalized using the free-stream dynamic pressure, is plotted in figure 9 as a function of distance from the step x. Figure 9(*a*) shows the disturbances produced by the steps as a function of x/δ. Far upstream of the step location levels are flat at 0.0112 and 0.0106 for the 30 and 60 m s^{-1} cases, respectively. As the boundary layer begins to experience the adverse pressure gradient levels begin to rise at an increasing rate (see the inset to figure 9*a*). The upstream influence clearly increases dramatically with step size as does the magnitude of the rise. For the largest step, the r.m.s. reaches approximately 5 times its undisturbed value at the last upstream measurement station, one-third of a boundary layer thickness ahead of the step.

The primary separation region just downstream of the step is a strong source of new turbulence and thus very intense fluctuations are generated here that then decay with downstream distance. The maximum C_p' around the separation region is hard to discern given limited spatial resolution of the microphone locations close to the step, but peak values of 0.13–0.14 are measured for the medium and large step. At any given absolute downstream location the pressure disturbance increases dramatically with step size, as does the absolute distance over which it decays. When streamwise distance is normalized on step height, however, there is a close similarity between the behaviour of the disturbance produced by each of the steps, figure 9(*b*). This graph shows the excess r.m.s. pressure fluctuation produced by the step, plotted against x/h on a log–log scale. In this form the decay of the intensity for all of the steps falls into a single band which develops a near-constant slope downstream of the reattachment region (i.e. $x/h > 6$–8). Consistent with Ji & Wang's (2012) findings this slope is close to -1, although a close examination of the variations associated with each individual flow suggests a slightly higher value. For reasons that will become apparent below, we have chosen to identify this slope as $-7/6$.

https://doi.org/10.1017/jfm.2014.405 Published online by Cambridge University Press

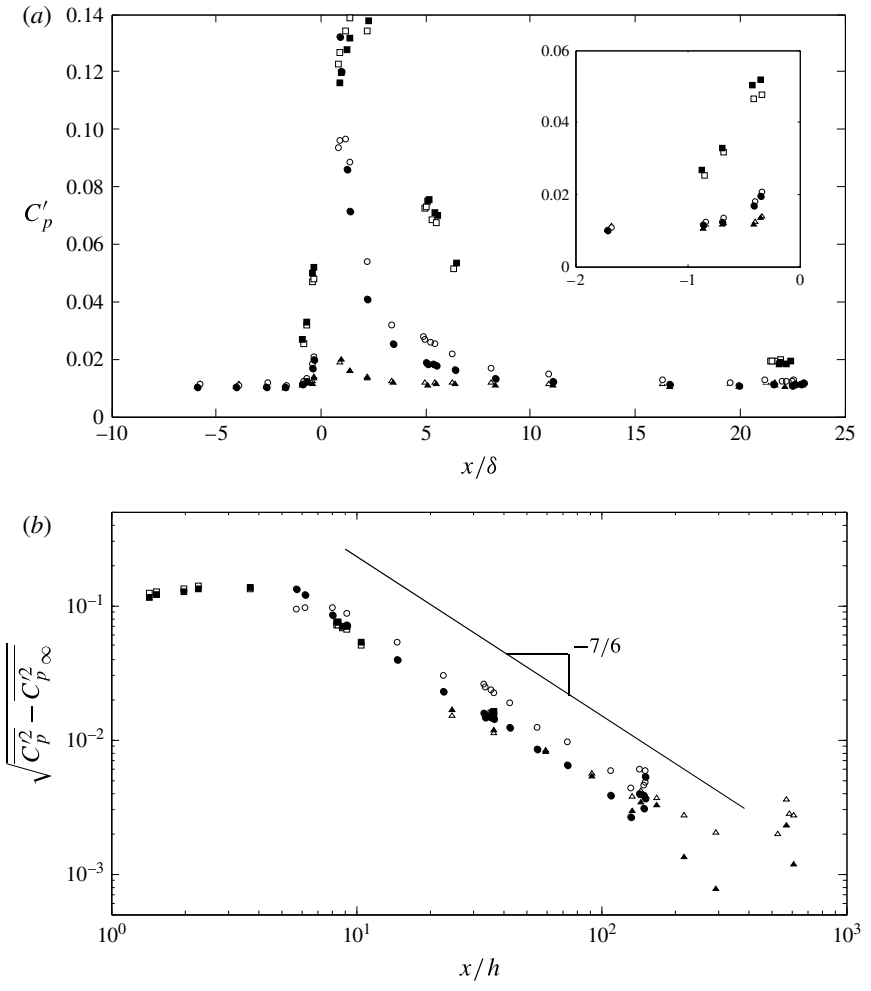


FIGURE 9. Root-mean-square pressure coefficient C'_p measured on the test wall for the three-step configurations. The legend is given in figure 8. (*a*) Dependence on x/δ (inset shows enlarged view of the region just upstream of the step location). (*b*) Dependence of the excess pressure fluctuation intensity, relative to the undisturbed mean square $\overline{C'^2_{p\infty}}$, on x/h.

3.2.2. *Autospectra*

Wall pressure spectra normalized by the undisturbed boundary layer thickness δ and free-stream velocity U_∞ are plotted in figures 10–12. Figure 10(*a*,*b*) show results for the smallest step ($h/\delta \sim 3.8\,\%$) at 30 and 60 m s^{-1}. The bottom half of these plots shows results measured upstream of the step, the top half shows results for downstream. Spectra are only plotted where the uncertainty in the acoustic subtracted data was less than 3 dB. The pressure spectrum of the undisturbed smooth wall boundary layer at the two speeds is shown by the bold black lines. This spectrum shows some characteristics typical of a zero-pressure-gradient turbulent boundary layer: a broad maximum at low frequency followed by an approximately straight 'overlap' region, with a slope of around −0.8, and finally a steep roll off with a

https://doi.org/10.1017/jfm.2014.405 Published online by Cambridge University Press

slope close to -5 (visible only at 30 m s^{-1}). According to theoretical arguments put forward by Bradshaw (1967) and Panton & Linebarger (1974), the overlap region that exists between low-frequency motions controlled by boundary layer scales and high-frequency motions controlled by viscous scales, should have a slope of -1. However, almost all previous studies (e.g. Blake 1970; McGrath & Simpson 1987; Goody 2004) show a slope of -0.7 to -0.8 in this region, consistent with the present measurements.

Far enough upstream of the step, the wall pressure spectrum is indistinguishable from its smooth wall form. The influence of the step first appears at $x/h = -18.1$ as an increase in the intensity of the pressure fluctuations below $f\delta/U_\infty = 0.1$. At this point, the mean pressure coefficient (figure 8) has increased to approximately 0.06, indicating a deceleration of the flow by a few per cent. At first sight this appears to be remarkably long reach for the step in the fluctuating pressure field, and one is reminded of the statement of Efimtsov *et al.* (1999) concerning small forward steps in subsonic and supersonic flow producing elevated pressure fluctuations as far as 100 step heights upstream. It is less surprising when one considers that 18 step heights is still significantly less than one boundary layer thickness, and thus the size of the largest eddies. The fact that the increase in pressure fluctuations is seen to extend to the lowest frequencies suggests that these largest eddies are involved, perhaps through their inviscid interaction with the step.

Moving closer to the step, low frequency spectral levels continue to rise and by $x/h = -9$ they are as much as 12 dB above smooth wall levels at the lowest frequencies. Here the influence of the step is felt up to a frequency $f\delta/U_\infty$ of approximately 1 and the maximum spectral level is found at $f\delta/U_\infty \cong 0.03$ or $fh/U_\infty \cong 0.0012$. Normalized on step height this is an order of magnitude lower than the low-frequency fluctuations (at $fh/U_\infty \cong 0.01$) seen by Camussi *et al.* (2008) ahead of their step. Normalized on incoming boundary layer thickness, however (giving $f\delta/U_\infty \cong 0.04$ in Camussi *et al.*'s case), these results are much closer, suggesting that these fluctuations may be as much to do with the unsteadiness of the incoming boundary layer turbulence as the dynamics of the step flow itself.

Comparing figure 10(*a*,*b*) for locations upstream of the step we see little effect of a doubling of the Reynolds number other than a slight increase (of 1 dB or less) in the low-frequency levels produced by the step. Note that the high-frequency limit on the pressure fluctuation measurements (of 20 kHz) is responsible for clipping the high-frequency portion of the surface pressure spectra measured at 60 m s^{-1} at the beginning of the roll-off region.

The evolution of the pressure spectrum downstream of the step is visible in the top half of figure 10. At the first measurement station, 24.7 step heights and about 6 reattachment lengths downstream, the effects of the step are felt through an increase in pressure fluctuations at all but the highest frequencies $f\delta/U_\infty < 50$. The increase is focused on shallow ridge centred at about $f\delta/U_\infty = 2$ ($fh/U_\infty = 0.08, fx_r/U_\infty = 0.18$). Moving downstream, the centre frequency of this feature and the spectral levels associated with it both gradually decay, and it becomes indistinguishable from the rest of the spectrum at around $x/h = 150$. Presumably, the increase in pressure fluctuations is associated with the additional turbulence generated in the primary separation region: the frequency of the ridge identifying the scale of the most energetic motions, governed by the shedding from that bubble. Far downstream of the step the spectral shapes do not quite return to their undisturbed form, although the residual differences may not be significant (note the slightly elevated levels around $f\delta/U_\infty = 0.3$ even at $x/h = 607$). Comparing the 30 and 60 m s^{-1} cases

https://doi.org/10.1017/jfm.2014.405 Published online by Cambridge University Press

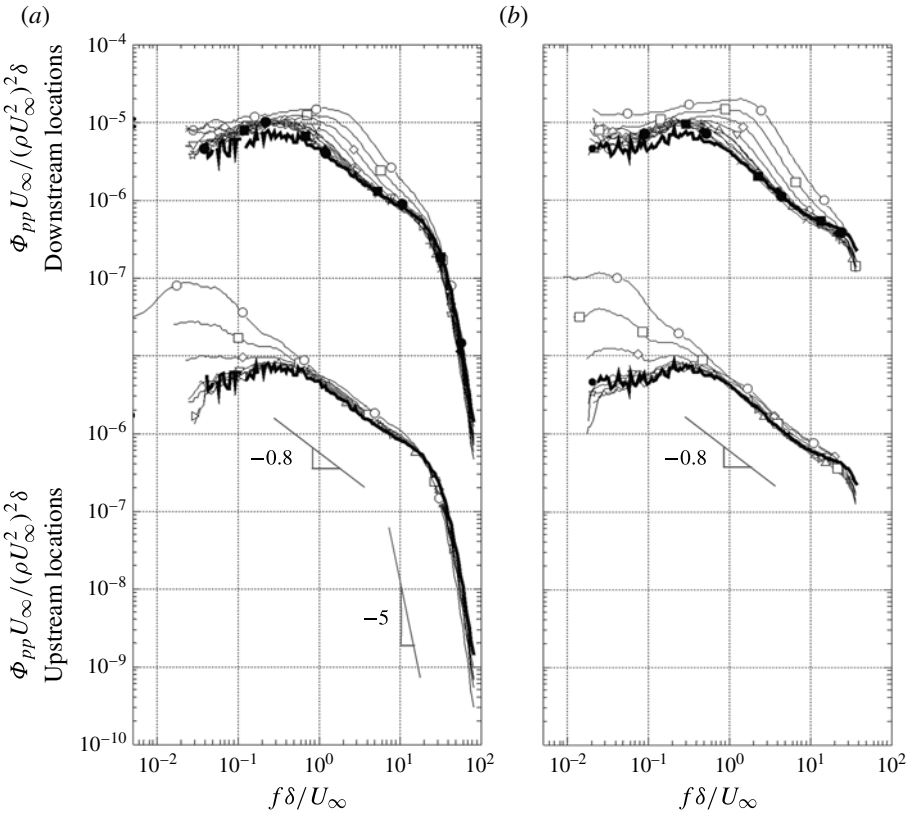


FIGURE 10. Surface pressure spectra measured with the 3.7 mm step at (*a*) 30 m s^{-1} and (*b*) 60 m s^{-1}. Downstream locations: ○, $x/h=24.7$; □, 36.4; ◇, 59.0; ▽, 91.2; △, 134; ◁, 146; ▷, 169; ✯, 219; +, 292; ×, 438; ✱, 526; ●, 573; ■, 584; ◆, 607; ——, undisturbed. Upstream locations: ○, $x/h=-9.0$; □, −10.8; ◇, −18.1; ▽, −22.6; △, −45.2; ◁, −68.6; ▷, −106; ✯, −156; ——, undisturbed.

(figure 10*a*,*b*) we see no qualitative effect of Reynolds number. Quantitatively, there is a slight increase (1–2 dB) in the excess pressure fluctuations generated by the step at low frequencies.

The effects of the two fourfold increases in the step size can be seen by comparing figures 10–12. These three figures show, for the most part, pressure fluctuation measurements at the same absolute stations (i.e. x/δ) and thus as the step height is changed they show different ranges of x/h. However, the factor of 4 ratio used in positioning of the microphones downstream of the step position ensure that many of these positions remain comparable in terms of x/h.

The flow approaching the medium step (figure 11*a*,*b*, $h/\delta\sim15\,\%$) shows an increase in the intensity of low-frequency pressure fluctuations that is qualitatively similar to that seen for the small step. There are important quantitative differences though. In particular, there is no clear effect of the step on the spectrum until about $x/h=-5.7$, where the disturbance to the mean pressure is about $0.15C_p$. Relative to its height the forward reach of the medium step appears one-third to one-half that of the small step with, for example, low-frequency spectral levels at $x/h=-4.5$ for the medium step being similar to those seen at $x/h=-9$ with the small step. Moving closer to

https://doi.org/10.1017/jfm.2014.405 Published online by Cambridge University Press

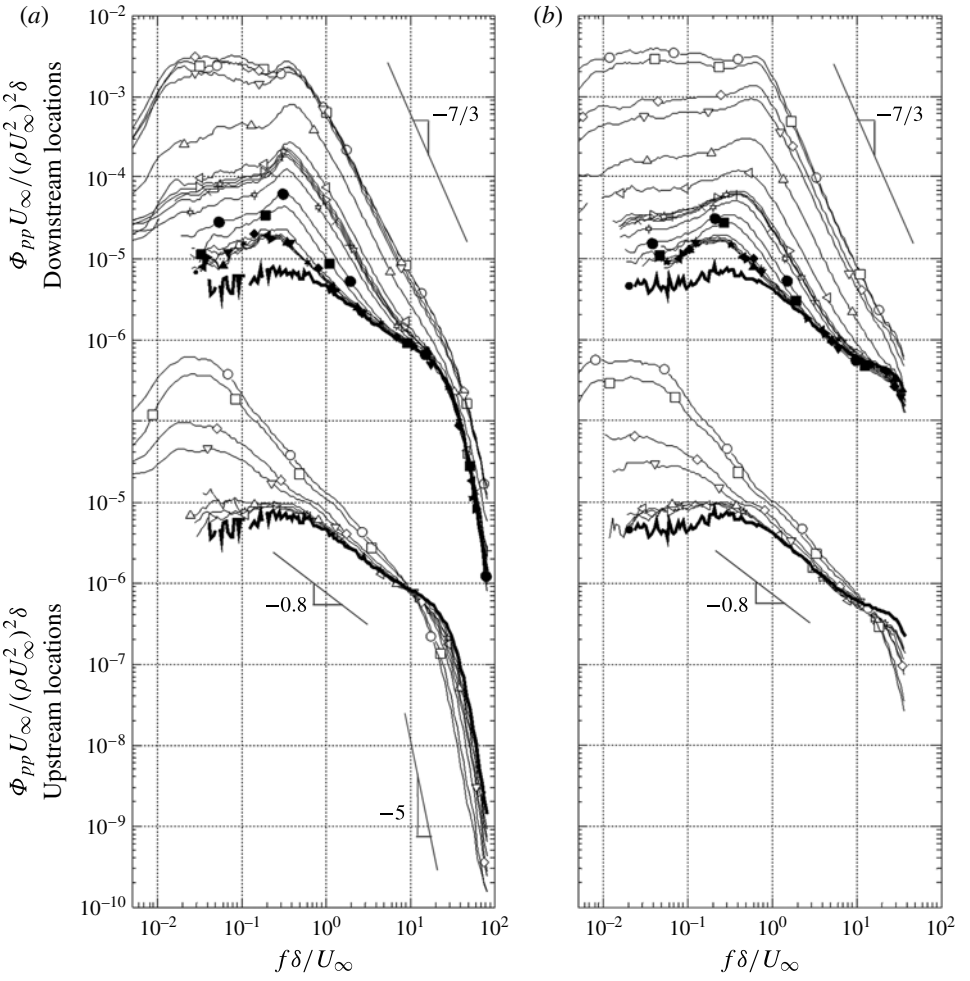


FIGURE 11. Surface pressure spectra measured with the 14.6 mm step at (*a*) 30 m s^{-1} and (*b*) 60 m s^{-1}. Downstream locations: ○, $x/h = 5.7$; □, 6.2; ◇, 8.0; ▽, 9.1; △, 14.8; ◁, 22.8; ▷, 33.1; ✯, 33.6; +, 35.4; ×, 36.5; ✲, 42.2; ●, 54.8; ■, 73.1; ♦, 109.6; ▼, 131.4; ▲, 142.7; ◀, 148.4; ▶, 149.5; ★, 151.3; ★, 151.7; ——, undisturbed. Upstream locations: ○, $x/h = -2.3$; □, −2.7; ◇, −4.5; ▽, −5.7; △, −11.3; ◁, −17.1; ▷, −26.6; ✯, −39.1; ——, undisturbed.

the medium step, low-frequency levels continue to rise and by the last measurement station at $x/h = -2.3$ are as much as 100 times as intense as those seen in the undisturbed boundary layer. This position is just upstream of the forward separation location for this step (see table 2) and so this may reflect long time scales associated with this separation bubble. The lifting of the flow (and of the small turbulent scales) away from the wall as part of this separation likely also explains the reduction in high-frequency ($f\delta/U_\infty > 10$) pressure fluctuations seen here.

The first measurement stations downstream of the medium step from $x/h = 5.7$ to 9.1 occupy the region just downstream of reattachment (see the top of figure 11). The pressure spectra here, which are all quite similar, show relatively intense pressure fluctuations over the entire measured frequency range. At low frequencies $f\delta/U_\infty < 0.5$

https://doi.org/10.1017/jfm.2014.405 Published online by Cambridge University Press

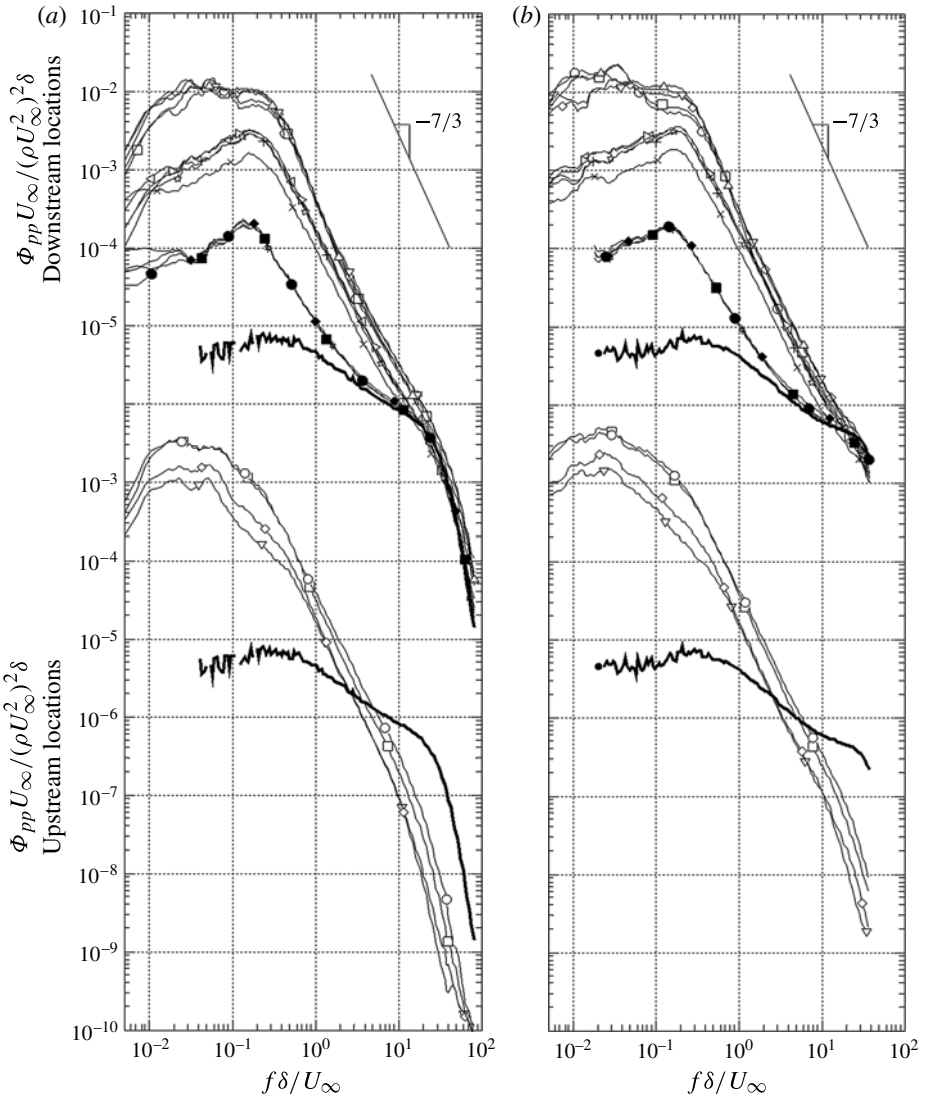


FIGURE 12. Surface pressure spectra measured with the 58.4 mm step at (*a*) 30 m s^{-1} and (*b*) and 60 m s^{-1}. Downstream locations: ○, $x/h = 1.4$; □, 1.5; ◇, 2.0; ▽, 2.3; △, 3.7; ◁, 8.3; ▷, 8.4; ✯, 8.8; +, 9.1; ×, 10.5; ✱, 35.7; ●, 35.8; ■, 36.2; ◆, 36.5; ——, undisturbed. Upstream locations: ○, $x/h = -0.6$; □, −0.7; ◇, −1.1; ▽, −1.4; ——, undisturbed.

spectral levels are roughly constant and almost three orders of magnitude larger than those seen in the undisturbed boundary layer. This plateau region is terminated at its high-frequency end by the same shallow ridge seen in the pressure spectra downstream of the smallest step. The ridge is centred at $f\delta/U_\infty = 0.5$ ($fh/U_\infty = 0.08, fx_r/U_\infty = 0.29$) and $f\delta/U_\infty = 0.8$ ($fh/U_\infty = 0.12, fx_r/U_\infty = 0.44$) for the 30 and 60 m s^{-1} cases, respectively, and is followed by a roll off in spectral levels with an almost constant slope of approximately −7/3. Despite this rapid drop, levels remain well above

https://doi.org/10.1017/jfm.2014.405 Published online by Cambridge University Press

those of the undisturbed boundary layer even at the highest frequencies measured ($f\delta/U_\infty = 40$–80).

The $-7/3$ power-law dependence may provide an important clue to the physics of the disturbance generated by the step. Pressure spectra with this behaviour have been seen previously in wall pressure fluctuations measured downstream of reattachment in a backstep flows by Lee & Sung (2001) and Camussi, Guj & Ragni (2006). Fundamentally, a $-7/3$ region is expected in the inertial subrange of the pressure spectrum of homogeneous isotropic turbulence in the limit of infinite Reynolds number (Batchelor 1953). It is also expected and has been observed in free shear flows (George, Beuther & Arndt 1984) where the generation of pressure fluctuations through turbulence–turbulence interactions dominates over that produced by turbulence–mean-shear interactions. The intriguing implication for the present flow is that the formation of a $-7/3$ region may indicate that in this spectral region the turbulence produced by the step is behaving more like that of a free shear flow (i.e. a wake) than that the boundary layer in which it is embedded.

Moving downstream the additional turbulence generated by the step decays in intensity and grows in scale. The portion of the pressure spectrum for which the step is responsible thus reduces in level and frequency, shifting downward and to the left in figure 11(*a*,*b*). The drop in spectral levels stops when they reach those of the undisturbed boundary layer. This recovery is first completed at the highest frequencies, near $x/h = 22.8$. It then progresses downward in frequency with distance downstream. By $x/h = 36$ the spectrum has recovered to its smooth-wall form at non-dimensional frequencies greater than approximately 10. Below this, the low-frequency ridge generated by the step is still very much in evidence, centred near $f\delta/U_\infty = 0.4$ ($fh/U_\infty = 0.06$, $fx_r/U_\infty = 0.22$) at 30 m s^{-1} and $f\delta/U_\infty = 0.5$ ($fh/U_\infty = 0.08$, $fx_r/U_\infty = 0.30$) at 60 m s^{-1}. At these frequencies, spectral levels are approximately 15 and 10 dB above those for the undisturbed boundary layer, respectively. The disturbance to the boundary layer is considerably greater than that seen at the same relative location ($x/h = 36$) downstream of the small step, and the frequencies associated with it are three to four times smaller, implying an approximate scaling on step height.

The decay continues with further distance downstream but at a decreasing and remarkably slow pace. At the last measurement station, 152 step heights downstream, the spectrum has relaxed to its undisturbed state at non-dimensional frequencies $f\delta/U_\infty$ above approximately 1. Below this frequency the ridge is still very much in evidence and is centred near $f\delta/U_\infty = 0.3$ ($fh/U_\infty = 0.05$, $fx_r/U_\infty = 0.18$), where spectral levels at both speeds are still half a decade (approximately 3 times) greater than those seen without the step.

The behaviour of the largest step flow ($h/\delta \sim 60\,\%$) seen from the perspective of the wall pressure spectrum (figure 12*a*,*b*) is qualitatively quite similar to that of the medium step. For the largest step, all of the upstream measurement stations are very close to the step ($x/h = -1.4$ to -0.6) and well within the forward separation bubble. We see here both a dramatic enhancement of low-frequency spectral levels ($f\delta/U_\infty < 3$) and suppression of high-frequency levels associated with this separation region. Interestingly, the intensity of both low- and high-frequency pressure fluctuations shows some increase with distance downstream within the bubble.

Downstream of the step, the spectra show the same low-frequency plateau, ridge and $-7/3$ roll off seen with the medium step, except shifted to lower frequencies. At $x/h = 9$ the ridge is centered near $f\delta/U_\infty = 0.2$ ($fh/U_\infty = 0.12$, $fx_r/U_\infty = 0.50$) for both flow speeds. At $x/h = 36$ this frequency is about 0.15 ($fh/U_\infty = 0.09$, $fx_r/U_\infty = 0.37$).

https://doi.org/10.1017/jfm.2014.405 Published online by Cambridge University Press

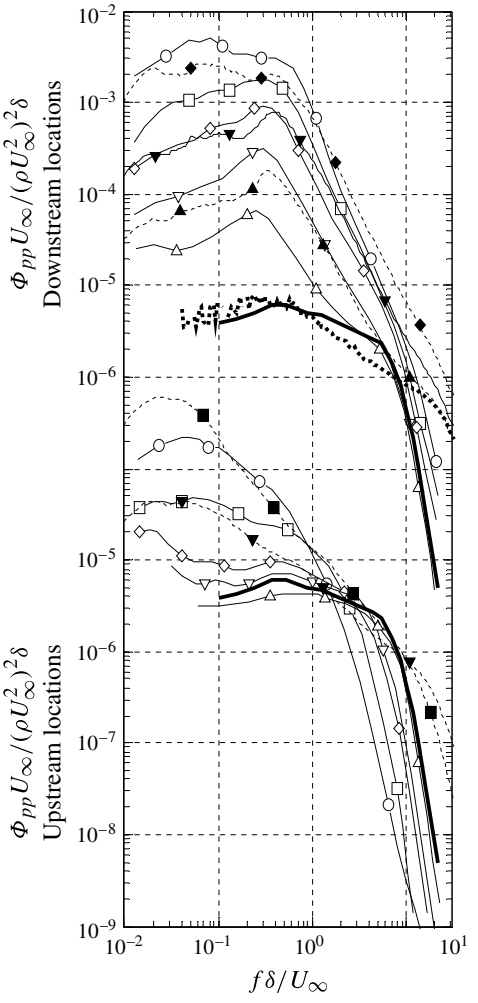


FIGURE 13. Surface pressure spectral data from Farabee & Casarella (1986) for $Re_h = 21\,000$, $h/\delta = 42\,\%$, compared with results for the 14.6 mm step at 30 m s^{-1} ($Re_h = 21\,000$, $h/\delta = 15.1\,\%$). Downstream locations. F&C: ○, $x/h = 2$; □, 4; ◇, 6; ▽, 12; △, 36; ——, undisturbed. Present data: ◆, $x/h = 5.7$; ▼, 14.8; ▲, 36.5; ·····, undisturbed. Upstream locations. F&C: ○, $x/h = -1$; □, -2; ◇, -3; ▽, -6; △, -16; ——, undisturbed. Present data: ■, $x/h = -2.3$; ▼, -5.7.

Note that when normalized on step height, these frequencies are almost the same as those seen for the medium and small steps at the same x/h positions, reinforcing the idea of a turbulence structure that is scaling on step size rather than boundary layer thickness. The rate of decay of the intensity of the excess pressure fluctuations is quite consistent between the medium and large steps, which both show about a 12 dB reduction between $x/h = 9$ and 36.

Figures 13 and 14 show comparisons of the present measurements with experimental results from Farabee & Casarella (1986) and data from Ji & Wang's (2010, 2012) large eddy simulations. Farabee and Cassarella's measurements (figure 13) were made for a single step height and Reynolds number. The relative size of their step

https://doi.org/10.1017/jfm.2014.405 Published online by Cambridge University Press

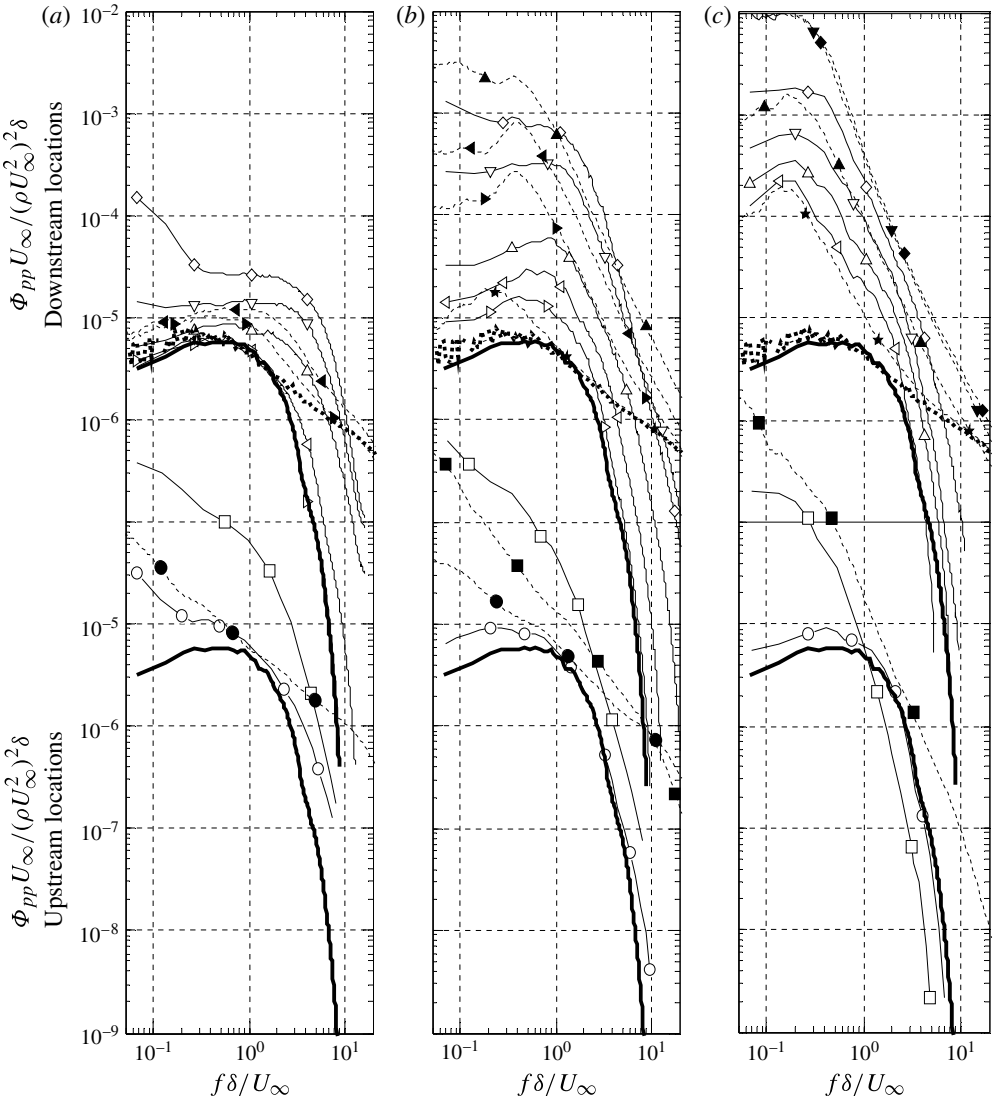


FIGURE 14. Surface pressure spectral data from Ji & Wang (2010, 2012) compared with the present results. (*a*) J&W, $Re_h = 1600$, $h/\delta = 3.3\,\%$: ○, $x/h = -6$; □, -1; ◇, 3; ▽, 6; △, 10; ◁, 40; ▷, 100; ——, undisturbed. Present, $Re_h = 6640$, $h/\delta = 3.8\,\%$: ●, $x/h = -9$; ◀, 36.4; ▶, 91.2; ·····, undisturbed. (*b*) J&W, $Re_h = 6400$, $h/\delta = 13\,\%$: ○, $x/h = -6$; □, -1; ◇, 1.5; ▽, 3; △, 7; ◁, 12.5; ▷, 25; ——, undisturbed. Present, $Re_h = 26\,600$, $h/\delta = 15.1\,\%$; ●, $x/h = -5.7$; ■, -2.3; ▲, 6.2; ◀, 14.8; ▶, 22.8; ★, 149.5; ·····, undisturbed. (*c*) J&W, $Re_h = 26\,000$, $h/\delta = 53\,\%$: ○, $x/h = -6$; □, -1; ◇, 1.7; ▽, 3.4; △, 10; ◁, 16; ——, undisturbed. Present, $Re_h = 106\,000$, $h/\delta = 58.3\,\%$: ■, $x/h = -1.1$; ◆, 2; ▼, 3.7; ▲, 10.5; ★, 36.2; ·····, undisturbed.

$h/\delta = 42\,\%$ is closest to that of the largest of the present steps (compare with figure 12*a*). Their step Reynolds number, of 21 000, is closest to that of the medium step at 30 m s^{-1} (compared directly in figure 13). Note that Farabee & Casarella's (1986) undisturbed boundary layer wall pressure spectrum had a comparatively shallow

https://doi.org/10.1017/jfm.2014.405 Published online by Cambridge University Press

overlap region with a slope of approximately -0.5 as compared with the present flow and most equilibrium boundary layer studies, see figure 13. Keeping the differences in flow conditions in mind, these data sets appear at least qualitatively consistent. Spectra measured inside the separation region just upstream of the largest step (figure 12*a*) are similar in shape and level to those measured at comparable locations by Farabee and Cassarella. Low-frequency spectral levels are somewhat greater in the present measurements, perhaps reflecting the higher Reynolds number. Compared with the medium step (included directly in figure 13) the rise in low-frequency spectral levels as the step is approached is quite closely mirrored in Farabee and Cassarella's data. However, this rise occurs further downstream in their flow, consistent with the larger h/δ and the trend already seen in the results for the small and medium steps of the present experiment. Downstream of the step Farabee and Cassarella's spectra have the same shape as the present results, including the ridge associated with the step generated turbulence and the $-7/3$ roll off on its high-frequency side. Looking at $x/h = 36$, the ridge in Farabee and Cassarella's spectra occurs at a non-dimensional frequency of about $f\delta/U_\infty = 0.3$ ($fh/U_\infty = 0.12, fx_r/U_\infty = 0.4$) fairly consistent with the scaling on step height proposed above. At this position the low-frequency shape of Farabee and Cassarella's spectrum is almost identical to that seen in the present measurements, although the spectral levels here are a few decibels lower than seen in the present flows at the most closely matching conditions.

The results of Ji & Wang's (2010, 2012) calculations (for step height ratios $h/\delta = 3.3$, 13.3 and 53.3 %) are plotted along with some of the present results for the corresponding step sizes in figure 14. Ji and Wang's large eddy simulation would not have resolved the smaller scales. Judging by the comparison between undisturbed boundary layer pressure spectra (figure 14) this appears to have affected the pressure spectrum at frequencies $f\delta/U_\infty$ down to approximately 2, although this limit would likely be higher for locations close to the step where grid refinement resulted in better resolution. We therefore confine our comments to observations on the lower-frequency end of the spectrum.

In the flow approaching the steps, Ji and Wang's results show the same enhancement of low-frequency pressure fluctuations seen in the present results. In the two cases where there is a close match in the locations (near $x/h = -6$ for the medium step, figure 11, $x/h = -1$ for the largest step, figure 12), the present measurements show spectral levels that are approximately 5 dB higher, however. A qualitative comparison of the flow downstream of the steps, shows quite good agreement in the low-frequency spectral shape and the manner of the decay with downstream distance. Quantitatively, however, levels are substantially lower and their rate of decay is faster in the calculation than the experiment. For the small step (figure 10) the calculations show the effects of the step to have almost completely disappeared by $x/h = 40$, whereas the measurements at $x/h = 36$ show the pressure fluctuations to be elevated across the frequency range and as much as 8 dB higher than in the undisturbed boundary layer. Similarly in the medium step flow, the calculations show about the same decay in spectral levels to $x/h = 25$ that the measurements show to $x/h = 150$.

A better quantitative agreement between the measurements and calculations of the pressure spectra downstream of the step (with spectral levels normalized on δ) can be obtained by comparing measurements at the same step Reynolds number, rather than at the same step height to boundary layer thickness ratio. Consider, for example, the close similarity between Ji and Wang's results for the largest step at $x/h = 16$ (figure 14*c*, $\triangleleft$) and the present measurements at $x/h = 14.8$ for the medium step (figure 14*b* $\blacktriangleleft$). Likewise, one can compare Ji and Wang's data for the medium step at $x/h = 25$ (figure 14*b* $\triangleright$) with the measurements for the small step at $x/h = 36.4$ (figure 14*a*, $\blacktriangleleft$).

https://doi.org/10.1017/jfm.2014.405 Published online by Cambridge University Press

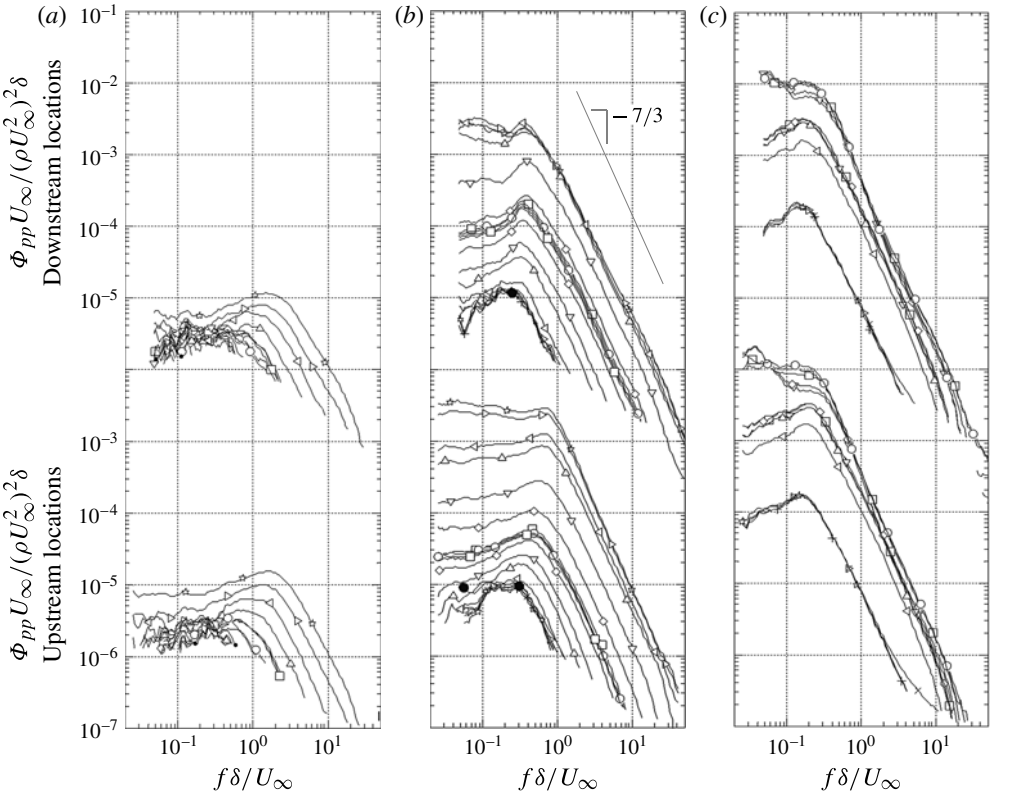


FIGURE 15. Disturbance pressure spectra measured with (*a*) the 3.7 mm step, (*b*) the 14.6 mm step and (*c*) the 58.4 mm step. Legends for parts (*a–c*) given in figures 10–12, respectively.

3.2.3. *Spectral scaling*

A particularly interesting feature of the flow downstream of the steps is that there are no locations where pressure fluctuation levels at any measured frequency fall significantly below levels for the undisturbed boundary layer (see figures 10–12). One expects that nonlinear processes in the step flow and its recovery would interfere with the boundary layer mechanics and suppress pressure fluctuations at some frequencies while enhancing them at others. However, this does not happen. It is as though the step generates a turbulent flow that is superimposed upon the boundary layer structure and decays independently of it. This is of course consistent with the observation, based on the reattachment length measurements of figure 7, that the step flow depends only weakly on h/δ. It is also consistent with the idea that the $-7/3$rds slope of the wall pressure spectrum is an indicator that the step disturbance is evolving like a free wake.

Taking this interpretation literally, we have re-plotted all of the spectra measured downstream of the steps in figure 15, but with the undisturbed boundary spectral levels at each frequency subtracted out. These disturbance spectra are only plotted for frequencies where spectral levels with the step were more than 1 dB greater than those without. The subtraction process markedly extends the linear $-7/3$ roll off region, resulting in a spectra that appear very similar in shape at different locations, different

https://doi.org/10.1017/jfm.2014.405 Published online by Cambridge University Press

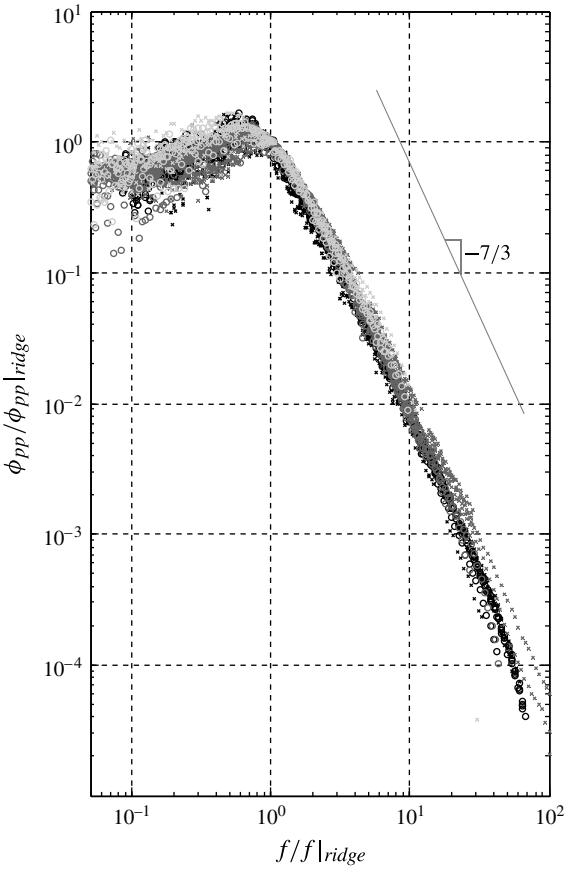


FIGURE 16. Disturbance pressure spectra normalized on the ridge frequency and spectral level for all measured cases and $x/h > 8$: ×, 58.4 mm step, 30 m s^{-1}; ○, 58.4 mm step, 60 m s^{-1}; ×, 14.6 mm step, 30 m s^{-1}; ○, 14.6 mm step, 60 m s^{-1}; ×, 3.7 mm step, 30 m s^{-1}; ○, 3.7 mm step, 60 m s^{-1}.

speeds and even different step heights. The only exception is those spectra measured close to the separated flow and reattachment regions $0 < x/h < 8$. Which show higher levels at low frequencies and a slightly more rapid roll off at high frequencies.

Just how similar the disturbance spectra measured downstream of $x/h = 8$ are, becomes clear if they are all plotted normalized on the frequency and spectral level of the ridge, $f|_{ridge}$ and $\phi_{pp}|_{ridge}$ (see figure 16). Since the ridge does not have a clear maximum in all cases, $f|_{ridge}$ and $\phi_{pp}|_{ridge}$ are defined in terms of the point where the slope of the spectrum passes through -1. The spectra closely follow the same curve, to within ± 1.5 dB at frequencies above that of the ridge. Spectra for the different step sizes are plotted in different shades of grey in figure 16, so it can be seen that there is no significant difference in the normalized form of the disturbance spectra produced by different step sizes. We therefore conclude that there is self-similarity in the disturbance spectrum not just within each flow but also between the different step flows.

Figure 17 shows the dependence of the similarity parameters, $f|_{ridge}$ and $\phi_{pp}|_{ridge}$, on streamwise position, Reynolds number and flow speed. Both parameters decrease

https://doi.org/10.1017/jfm.2014.405 Published online by Cambridge University Press

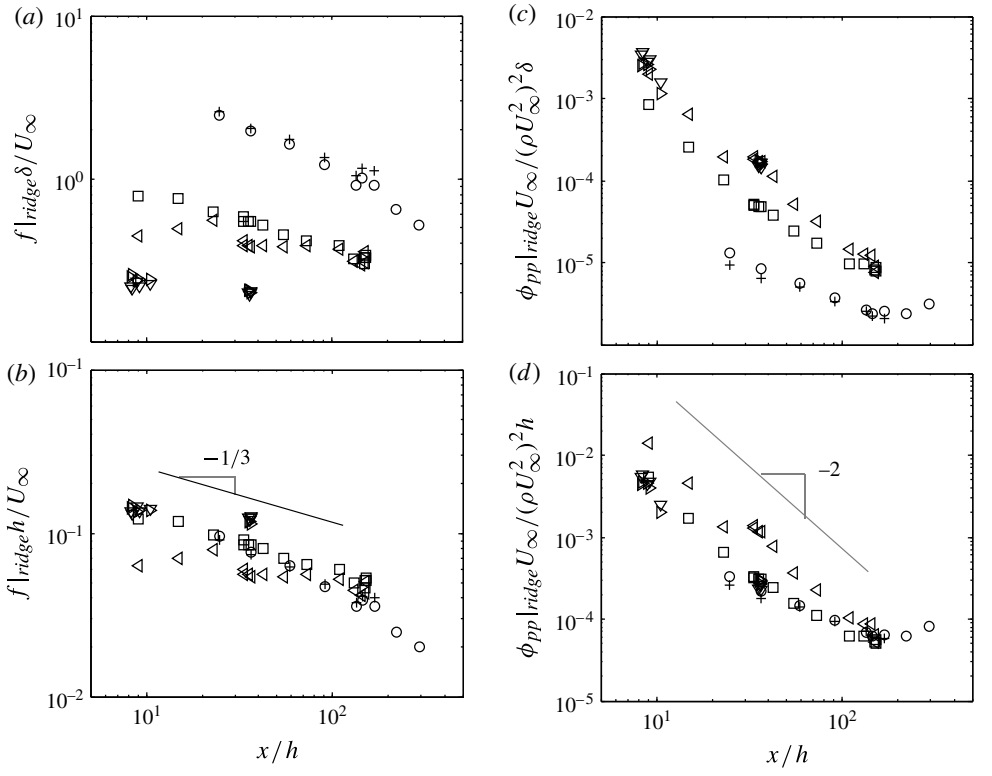


FIGURE 17. Ridge frequency and spectral level as a function of x/h. (*a*) Ridge frequencies normalized on incoming boundary layer thickness and (*b*) normalized on step height. (*c*) Ridge spectral level normalized on boundary layer thickness and (*d*) normalized on step height, with: ▷, 58.4 mm step, 30 m s^{-1}; ▽, 58.4 mm step, 60 m s^{-1}; ◁, 14.6 mm step, 30 m s^{-1}; □, 14.6 mm step, 60 m s^{-1}; +, 3.7 mm step, 30 m s^{-1}; ○, 3.7 mm step, 60 m s^{-1}.

with downstream distance and follow quite different trajectories for the three step sizes when these parameters are normalized on boundary layer thickness and free-stream velocity (figure 17*a*,*c*). Normalizing on step height and free-stream velocity (figure 17*b*,*d*), however, quite successfully collapses the variations of both parameters. We see that $f|_{ridge}h/U_\infty$ varies approximately as $(x/h)^{-1/3}$ and $\phi_{pp}|_{ridge}U_\infty/(\rho U_\infty^2)^2h$ varies approximately as $(x/h)^{-2}$, in both cases independent of Reynolds number. Note that a similar correlation of the parameters measured with different step heights can be obtained by normalizing $f|_{ridge}$ and $\phi_{pp}|_{ridge}$ on the reattachment length in place of the step height.

The scaling of the step disturbance spectral parameters on step height (or reattachment length) further bolsters the idea that the disturbance somehow decays independently of the boundary layer in which it is immersed. It also means that the disturbance produced by the different step sizes at the same relative location (e.g. $x/h = 36.5$), only appears different in figures 10–12 because the disturbances are of different intensity relative to the boundary layer in which they are growing. Each of these disturbance spectra has closely the same form, as evidenced by figures 15 and 16. Note that the dependence of the similarity parameters with x/h revealed in

https://doi.org/10.1017/jfm.2014.405 Published online by Cambridge University Press

figure 17(*b*,*d*) implies that the mean square of the pressure fluctuations associated with the step disturbance should vary as $(x/h)^{-7/3}$ as the disturbance decays. This is obviously consistent with the $(x/h)^{-7/6}$ dependence of the r.m.s. pressure fluctuations seen in figure 9(*b*).

It is interesting to postulate that the characteristics of pressure disturbance may be consistent with a random distribution of coherent structures shed from the separation bubble with an average passing frequency at given x location given by the ridge frequency. The time history of the surface pressure fluctuations would then be expected to scale as

$$p\,(x,\,t) = \frac{\rho \Gamma U_\infty}{L} F\left(\frac{U_c t}{L},\,\frac{L}{h}\right) \tag{3.1}$$

where Γ is the circulation induced by the coherent structure, U_c is its convection velocity, L is its physical size and $F()$ a non-dimensional function. The frequency spectrum would then scale as

$$\phi_{pp}(f) \propto \frac{U_c}{L}\left(\frac{\rho \Gamma U_\infty}{U_c}\right)^2 \left|\tilde{F}\left(\frac{fL}{U_c},\,\frac{L}{h}\right)\right|^2. \tag{3.2}$$

Comparing the group fL/U_c to the ridge frequency scaling revealed in figure 17 suggests that $(L/U_c)U_\infty/h \sim (x/h)^{1/3}$ indicating that the size of the structures is growing with downstream distance. Similarly, comparing the ϕ_{pp} expression above with the scaling of the ridge spectral level visible in figure 17 suggests that $\Gamma/\sqrt{LhU_cU_\infty} \sim (x/h)^{-1}$ and therefore $\Gamma/U_c h \sim (x/h)^{-5/6}$. Thus the structures must be declining in strength and/or convecting more quickly as they evolve downstream. It will be shown later that the convection velocity of the turbulence at the ridge frequency does indeed increase with distance downstream.

3.2.4. *Space–time correlations*

Pressure fluctuation cross-spectra measured with the five-microphone array and single additional microphone (figure 4) were processed to remove acoustic contamination, inverse-Fourier transformed to yield space–time correlations, and then interpolated to produce correlation maps. Spanwise and streamwise space–time correlation coefficient functions are shown in figures 18–20 for all three step heights and the undisturbed boundary layer. Results are only shown for 30 m s^{-1}, since those for 60 m s^{-1} are similar. Correlations are plotted as functions of spatial separation (Δx or Δy) normalized on the undisturbed boundary layer thickness and time delay t normalized on the free-stream velocity and boundary layer thickness. In order to show more of the time variation, most of the plots have been distorted so that the range of the time axis represents a convection distance equivalent to approximately three times the range of the Δx or Δy axes. Correlation functions for the undisturbed boundary layer are shown in figure 18, both distorted and undistorted, to show this effect. The blue tick marks to the right-hand side of the plots in figure 18 also show the spanwise and streamwise separations at which data were actually measured. Note that some of the contour levels close to zero correlation show weak organized features that are associated with uncertainty and interpolation bias that should not be confused with flow structure. Included here are the faint bands that appear horizontally and vertically in figure 18(*a*,*c*) and in parts of figure 19, and horizontally and diagonally in parts of figure 20, diagonal since interpolation for the streamwise correlation contours was performed on a grid skewed to match the slope of the convective ridge.

https://doi.org/10.1017/jfm.2014.405 Published online by Cambridge University Press

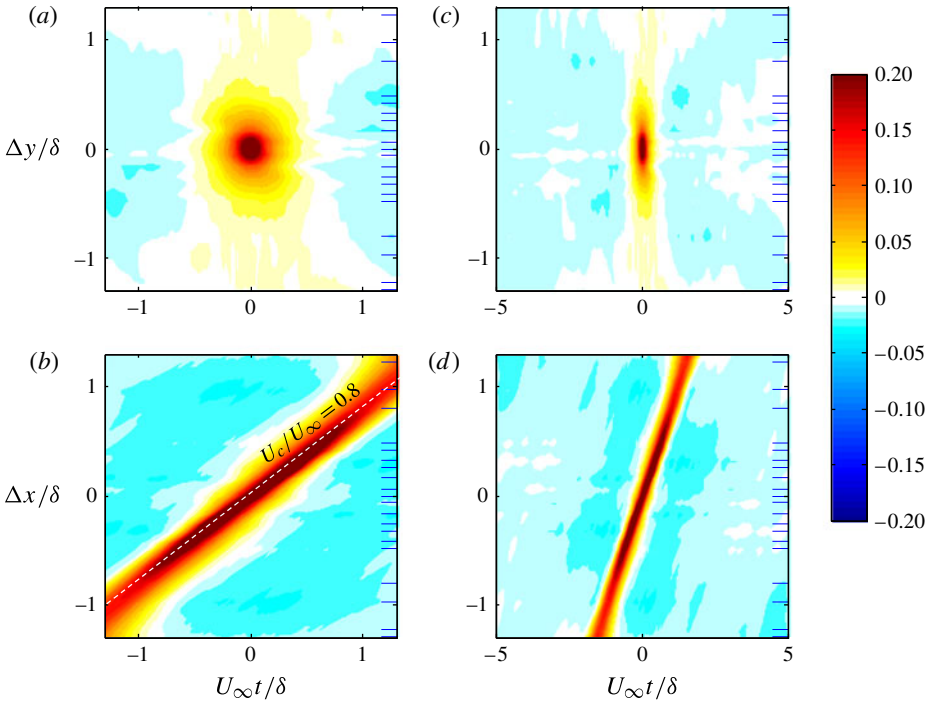


FIGURE 18. (*a*) Spanwise and (*b*) streamwise space–time pressure correlation coefficient functions for the undisturbed boundary layer at $U_\infty = 30$ m s^{-1}. (*c*) and (*d*) show the same data as (*a*) and (*b*) but on the distorted scales used in figures 15 and 16.

To create these pictures, the cross-correlations between all simultaneously measured microphones were calculated and then ordered by spatial separation. This procedure implicitly assumes statistical homogeneity in the direction of separation. This requirement is met in the spanwise direction through the two-dimensionality of the flow. It is also quite closely met in the streamwise direction for the locations downstream of the step, particularly for the medium- and large-scale steps where the streamwise variations occur on a scale that is long compared with the dimension of the array. It is not a good assumption upstream of the step, and thus streamwise space–time correlation functions are not shown here.

Consider first the streamwise correlation coefficient for the undisturbed boundary layer (bottom of figure 18) which clearly shows the convective ridge. A close-up view of the contours defining the ridge shows that it has a lower slope for small separations than for large ones, reflecting the fact that the large-scale pressure fluctuations tend to be associated with the bigger eddies that are carried along by the outer, faster moving part, of the boundary layer. On the largest scale the convection velocity appears to be close to 80 % of U_∞ in agreement with earlier studies (e.g. Blake 1970). Now turning to the undistorted view of the spanwise correlation coefficient (top of figure 18) we see a roughly oval distribution. This shows the correlation coefficient decaying to 5 % at a spanwise separation Δy of 0.35δ. In the time direction, the correlation decays to this level at $U_\infty t/\delta = 0.3$. Accounting for the large-scale convection velocity of $80\,\%U_\infty$ this makes the implied structure almost isotropic. In the distorted view this function appears as a much narrower spanwise strip.

https://doi.org/10.1017/jfm.2014.405 Published online by Cambridge University Press

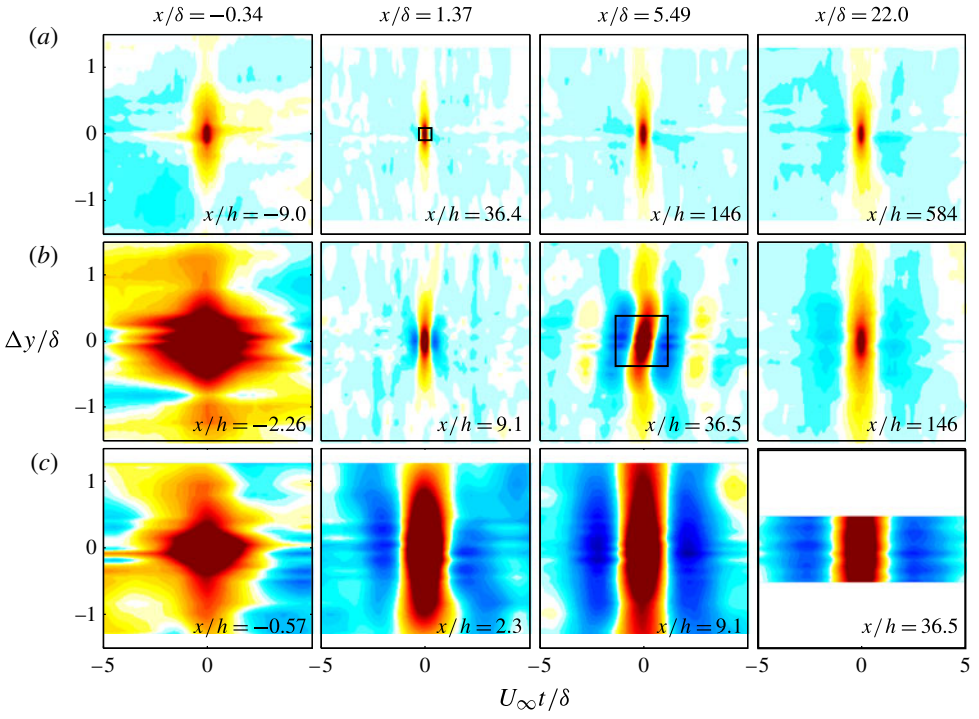


FIGURE 19. Spanwise space–time pressure correlation coefficient function at U_∞ = 30 m s^{-1}: (*a*), 3.7 mm step, $h/\delta = 3.8\,\%$; (*b*) 14.6 mm step, $h/\delta = 15.1\,\%$; (*c*) 58.3 mm step, $h/\delta = 60.1\,\%$. Undisturbed boundary layer results and colour scale shown in figure 18.

Consider now the correlation functions for the small step. Upstream of the step, at $x/h = -9$, the spanwise correlation function (figure 19*a*) has about twice the width in the time direction as the undisturbed boundary layer, and extends approximately 50 % further in the spanwise direction. This shows that the increase in low-frequency pressure fluctuations upstream of the step is associated with an increase in spanwise organization. Conversely, downstream of the step at $x/h = 36$ the spanwise and time-wise extent of the correlation function is reduced compared with the undisturbed boundary layer, implying that smaller-scale turbulence is primarily responsible for the enhanced pressure fluctuations seen here. By $x/h = 146$ the spanwise space–time correlation appears to have completely recovered its undisturbed form. A similar behaviour is seen in the streamwise correlation (figure 20) which at $x/h = 35$ shows a narrower convective ridge and a more rapid decay along the convective ridge, consistent with smaller, less-organized turbulence. By $x/h = 146$ the streamwise correlation too has returned to its undisturbed form.

Moving on to the medium step (figures 19*b* and 20*b*), the spanwise correlation shows a dramatic elongation in both time and spanwise directions at $x/h = -2.26$, suggesting the presence of nearly stationary spanwise organized disturbances in the flow approaching separation just upstream of the step. Downstream of the step the correlations initially appear to be recovering to their smooth wall values. At $x/h = 9$ the spanwise correlation function appears quite similar to that of the smooth wall except for slightly higher correlations along the spanwise axis, and the presence of

https://doi.org/10.1017/jfm.2014.405 Published online by Cambridge University Press

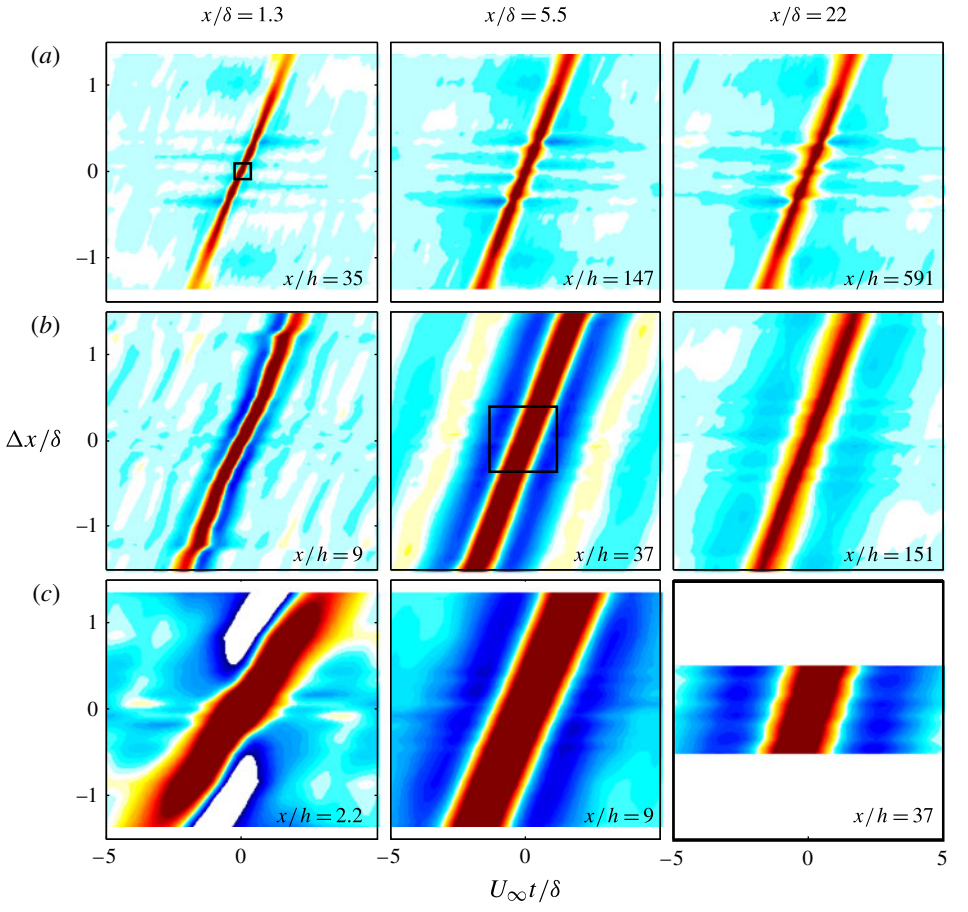


FIGURE 20. Streamwise space–time pressure correlation coefficient function at $U_\infty =$ 30 m s^{-1}: (*a*) 3.7 mm step, $h/\delta = 3.8\,\%$; (*b*) 14.6 mm step, $h/\delta = 15.1\,\%$; (*c*) 58.3 mm step, $h/\delta = 60.1\,\%$. Undisturbed boundary layer results and colour scale shown in figure 18.

two negative lobes to either side. The streamwise correlation function also shows these lobes, and a much more gradual decay of the correlation along the convective ridge (implying longer lasting turbulence) than in the undisturbed flow. The pressure correlation does not continue to progress towards its smooth wall form, however, and by $x/h = 37$ it has developed quite a different structure. The spanwise organization has grown and the correlation extends two to three times as far in the y direction as in the undisturbed boundary layer (figure 18). In the time-wise direction, an oscillatory structure has developed extending the time delay over which significant correlations are seen by an order of magnitude. The period of this oscillation is about $2.8\delta/U_\infty$ ($19h/U_\infty$, $5.3x_r/U_\infty$), implying a streamwise spacing between correlated structures of approximately 2.3 boundary layer thicknesses or 15 step heights. This time scale corresponds quite closely to the frequency of the ridge seen in the pressure spectra at this station (figure 11*a*), of $f\delta/U_\infty = 0.4$ ($fh/U_\infty = 0.06$, $fx_r/U_\infty = 0.22$). Given the frequencies involved it seems likely that the source of this organization is the shedding of large coherent eddies from the separation bubble downstream of the step.

https://doi.org/10.1017/jfm.2014.405 Published online by Cambridge University Press

Further downstream, near $x/h = 150$ the periodic structure has grown and partially decayed, but still dominates the outer reaches of the correlation function. The time scale has increased to about $4\delta/U_\infty$ ($26h/U_\infty$, $7.2x_r/U_\infty$) which is approximately consistent with the ridge in the pressure autospectra at $f\delta/U_\infty = 0.3$ ($fh/U_\infty = 0.05$, $fx_r/U_\infty = 0.18$) for this position (figure 11*a*). It is perhaps not so surprising that the step disturbs the flow over such a long streamwise distance, given the development of this large well-organized motion.

The measurements made with the large step (figures 19*c* and 20*c*) show even greater disturbance to the wall pressure field downstream of the step. The spanwise and streamwise correlation measurements near $x/h = 2.2$ are actually made within the region of separation and we see very large-scale spanwise and streamwise organization. The convective ridge shows that pressure disturbances are still traveling downstream here but with a convection velocity of only about $40\,\%U_\infty$. Further downstream a very organized quasiperiodic structure develops, much as seen with the medium step, but on a significantly larger scale. At $x/h = 9.1$ and 37 the correlation function extends well beyond the spanwise and streamwise limits of the measurement. The scale of the time-wise oscillations in the correlation function at $x/h = 9.1$ appears to be about $5\delta/U_\infty$ ($8h/U_\infty$), falling in line with the frequency of the ridge in the autospectra at this position at $f\delta/U_\infty = 0.2$.

The correlation functions for the different steps can be compared at the same values of x/h by looking diagonally across the grids of plots in figures 19 and 20. Such a comparison shows that, even with distances normalized on step height, the downstream influence of the step dramatically increases with h/δ. Based on our observations concerning the scaling of the time spectrum of wall pressure we would expect that this dramatic increase reflect the fact that the pressure disturbance scales primarily with the step size. We have added boxes to the correlation contours for the small and medium step for $x/h = 37$ in figures 19 and 20. These boxes are scaled so that, when normalized on step height h, they cover the same spanwise and time-wise distances as the entire plot shown for the largest step at $x/h = 37$. Comparing the contents of the boxes to the largest step correlations we do see an approximate scaling on step height, even though (unlike with the spectra) we have not attempted to subtract the presumed background contribution to the correlation from the undisturbed turbulent boundary layer.

3.2.5. *Convection velocities*

The streamwise space–time correlation data of figures 18 and 20 can also be studied in spectral form. Perhaps the most physically informative parameter that can be extracted is the phase convection velocity U_{cp}. This is given by the streamwise separation distance Δx divided by the time delay as a function of frequency, the time delay being obtained from the cross-spectral phase between the pressure fluctuations at the points separated by Δx. Figure 21 shows contours of phase velocity, as a function of frequency and Δx for each of the main measurement stations shown in figure 20 for the medium step and also for the undisturbed boundary layer. Plots for the small and large step show similar variations but are noisier. The vertical dashed lines included in the plots for the medium step show the ridge frequencies plotted in figure 17. Contours are only plotted where the coherence was greater than 0.05 and are most uncertain at low frequencies and separations where the phase delays are smallest, hence the spurious features on the lower left corners of the contour maps. Figure 22 shows the phase velocity at the ridge frequency, averaged with respect to Δx, as a function of streamwise position in each of the flows.

https://doi.org/10.1017/jfm.2014.405 Published online by Cambridge University Press

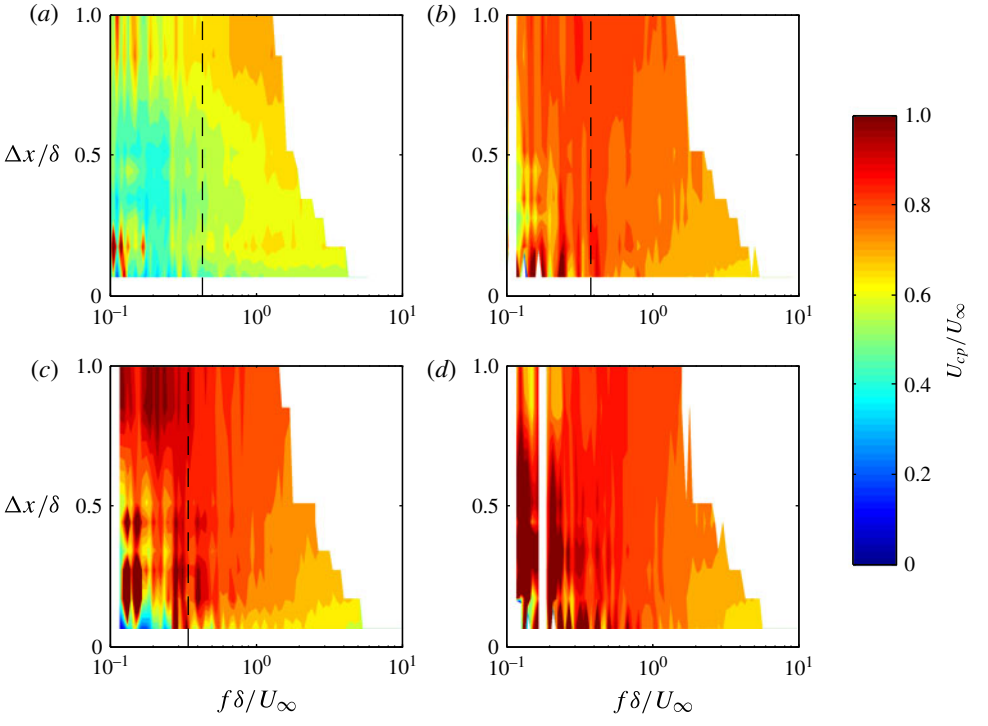


FIGURE 21. Phase convection velocity U_{cp} as a function of frequency and streamwise separation at $U_\infty = 30$ m s^{-1} for the 14.6 mm step, $h/\delta = 3.8\,\%$: (*a*) $x/h = 9$, (*b*) $x/h = 37$, (*c*) $x/h = 151$ and (*d*) undisturbed boundary layer. Vertical dashed lines show the ridge frequencies from figure 17.

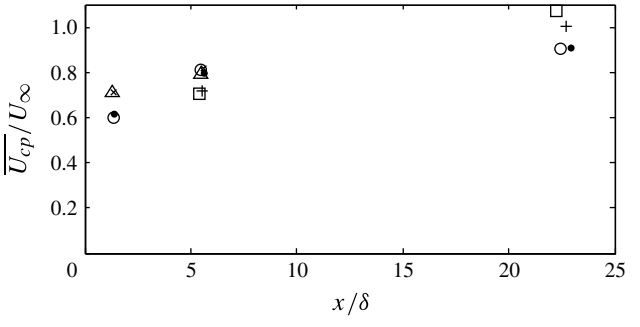


FIGURE 22. Phase convection velocity at $f|_{ridge}$, averaged over Δx, as a function of distance downstream of the step: results for 30 m s^{-1}: △, 3.6 mm step; ○, 14.4 mm step; □, 58.3 mm step. Results for 60 m s^{-1}: ×, 3.6 mm step; ●, 14.4 mm step; +, 58.3 mm step.

In the undisturbed boundary layer (figure 21*d*) the convection velocity for small separations $\Delta x < 0.3$ decreases gradually with frequency from about $0.9U_\infty$ for $f\delta/U_\infty \approx 0.25$ to around $0.65U_\infty$ for $f\delta/U_\infty \approx 5$: the highest frequency at which a significant coherence was measured. This dependence, which is quite typical for an equilibrium turbulent boundary layer (e.g. Blake 1970), is explained by the fact

https://doi.org/10.1017/jfm.2014.405 Published online by Cambridge University Press

that near-wall small-scale/high-frequency structures will tend to be convected more slowly than large-scale eddies that encompass the faster-moving outer region of the boundary layer. We see that the phase velocity does not vary strongly with streamwise separation Δx, but at high frequencies there is a discernable increase in U_{cp} with Δx. This is presumably because the higher-frequency fluctuations that correlate over large distances are more likely to be the result of non-sinusoidal components of large eddy pressure signals than due to small-scale structures.

Consider next the phase velocity maps in the wake of the step (see figure 21*a–c*). Around $x/h = 9$, not far downstream of reattachment, convection velocities are reduced compared with the equilibrium boundary layer, and their dependence with frequency reversed. Velocity is seen to increase with frequency from about $0.42U_\infty$ at $f\delta/U_\infty \approx 0.25$ to about $0.57U_\infty$ at $f\delta/U_\infty \approx 5$. This may indicate that large-scale organized eddies shed from the reattachment region are initially travelling slower than the rest of the boundary layer in which they are immersed. This would be an effect of the images of the eddies in the wall if those structures are initially located near the bottom of the boundary layer. Note that the overall low values of these convection velocities are consistent with previous observations made just downstream of reattachment in forward and backward facing step flows (e.g. Lee & Sung 2002; Camussi *et al.* 2008). Moving downstream we see the convection velocity at low frequencies progressively increases and by $x/h = 151$ the phase-velocity spectrum has almost recovered to its equilibrium form. The phase velocity distributions of figure 21 show no distinct features at the ridge frequencies (indicated by the vertical dashed lines). However, the convection velocity at those frequencies shows a clear increasing trend with downstream distance. This is shown for all of the flow cases in figure 22. Near $x/\delta = 1$ turbulent pressure fluctuations associated with the ridge are convecting downstream at 60–70 % of the free-stream velocity. By $x/\delta = 22$ the convection speed is all but indistinguishable from U_∞. This is consistent with our assertion, made in § 3.2.3 that the coherent structures producing the ridge are growing away from the wall as they convect downstream.

4. Conclusions

The effects of small forward facing steps upon the wall pressure fluctuations of a high-Reynolds-number turbulent boundary layer have been studied experimentally. Zero-pressure-gradient boundary layers of almost 100 mm thickness were generated on a test wall installed in a large-scale anechoic wind tunnel. The free-stream velocity was set to either 30 or 60 m s^{-1} producing undisturbed boundary layer momentum thickness Reynolds numbers of 15 500 and 26 600. Steps of 3.7, 14.6 and 58.4 mm were then introduced into the wall and the impact on the flow was studied. The implied step height to boundary layer thickness ratios were chosen to match large eddy simulations performed at lower Reynolds number by Ji & Wang (2010, 2012).

Mean surface pressures and oil flow visualizations were performed to examine the extent of the separated flow regions produced by the step. These measurements indicate an increase in reattachment length with Reynolds number that is particularly strong for the smallest step size. This explains the smaller reattachment lengths seen in Ji and Wang's large eddy simulations and perhaps the absence of a separation bubble altogether in their calculation for the small step. Step Reynolds number appears to be a more important factor than step height to boundary layer thickness ratio in determining the reattachment length.

Particular attention was paid to measurements of the fluctuating wall pressure field, which were examined from five boundary layer thicknesses upstream of the

https://doi.org/10.1017/jfm.2014.405 Published online by Cambridge University Press

steps to 22 boundary layer thicknesses downstream (over 600 step heights for the smallest step). As the boundary layer approaches the step low-frequency pressure fluctuations on the wall ($f\delta/U_\infty$ less than approximately 1) intensify and become more organized in the spanwise direction, increasing the overall r.m.s. pressure. The distance over which this forward influence acts is a function of step height to boundary layer thickness ratio h/δ, growing from approximately 6 step heights for $h/\delta = 15\,\%$ to $18h$ for $h/\delta = 3.8\,\%$. Immediately ahead of the step, where the flow separates, low-frequency pressure fluctuations develop a strong spanwise correlation and can exceed their undisturbed levels by over two orders of magnitude. In this region, higher-frequency fluctuations are suppressed as the forward separation lifts the small-scale turbulence away from the wall.

Separation of the flow from the salient edge of the step and the subsequent reattachment generate additional turbulence throughout the frequency range. Pressure fluctuations are most strongly enhanced at lower frequencies. Spectra develop a distinctive shape consisting of a low-frequency plateau and a roll off at higher frequencies with a near constant slope that approaches $-7/3$ as the step-size is increased. A ridge forms between these two features that defines the frequency scale of the step disturbance. At the same relative downstream position (x/h) the ridge frequency has a near-constant value when normalized on step height, fh/U_∞ being close to 0.08 at $x/h = 36$ for example, for all of the steps. Given the factor of 16 range in step sizes tested, this clearly indicates a turbulence structure that is scaling on the step geometry rather than boundary layer thickness.

As the flow progresses downstream the additional turbulent pressure fluctuations generated by the step decays in intensity and grows in scale, their r.m.s. contribution decaying at a rate closely proportional to $(x/h)^{-7/6}$. The excess portion of the pressure spectrum for which the step is responsible thus reduces in level and frequency. This decay stops when levels reach those of the undisturbed boundary layer. This recovery is first completed at the highest frequencies and then progresses down in frequency with distance downstream. For all of the steps, recovery at the highest frequencies $f\delta/U_\infty > 20$ occurs by $x/h = 30$. The decay continues after this but at a decreasing and remarkably slow pace. At 152 step heights downstream of the 14.6 mm step (the last measurement station) the step disturbance in the pressure spectrum is still obvious. The spectral ridge is clearly still visible centred at $fh/U_\infty = 0.05$ and spectral levels here remain about half a decade above those seen in the undisturbed boundary layer.

The disturbance to the pressure spectrum produced by the steps can be meaningfully separated by subtracting the undisturbed boundary layer pressure spectrum. This disturbance spectrum exhibits an extended roll of region of $-7/3$ slope. This may indicate that turbulence produced by the step is behaving more like that of a free shear flow (i.e. a wake) than that of the boundary layer in which it is embedded. The disturbance pressure spectrum also appears to be self-similar downstream of the reattachment region ($x/h > 8$) with a form almost independent of streamwise position, step size and Reynolds number. The frequency and amplitude scales of the disturbance spectrum appear to collapse to single-valued functions of x/h when normalized on step height (relative to boundary layer thickness) and free stream velocity, supporting the hypothesis that the step disturbance is somehow produced and decays independently of the boundary layer in which it is immersed. The frequency scale of the disturbance varies as $(x/h)^{-1/3}$, where as the spectral scale varies as $(x/h)^{-2}$, consistent with the decay rate of the excess r.m.s. pressure.

Spanwise and streamwise space–time correlations supply important clues to the physics behind the extraordinary persistence of the pressure disturbance. Measurements

https://doi.org/10.1017/jfm.2014.405 Published online by Cambridge University Press

made with the 14.6 mm step show that, well downstream of reattachment, the flow develops an organized quasiperiodic structure with a time scale that matches that of the ridge seen in the pressure spectra. The first signs of this structure, seen at $x/h = 9.1$, are negative lobes in the pressure correlations. The structure then grows in visibility and is most clear in measurements at $x/h = 37$. While it has begun to decay by $x/h = 146$ it still dominates the surface pressure correlation here, which remains very different to that of the undisturbed boundary layer. Comparisons with previous studies of the near-field structure of backstep flows suggests that this structure may be initiated by the regular formation of eddies in the separated flow at the step. It is therefore particularly interesting that it becomes most clearly visible in the surface pressure field some 10 reattachment lengths downstream. The coherence and scale of this motion, as seen in the wall pressure correlations, are a strong function of step height, relative to the boundary layer thickness, in a manner consistent with the idea that the step disturbance is almost independent of the incident boundary layer.

Acknowledgements

The authors would like to thank the Office of Naval Research, in particular Dr R. Joslin, for their support under grants N00014-09-1-0315 and N00014-12-1-0374. We would also like to thank Professor M. Wang and his research group for providing the results from their computations and for discussions of the above results.

REFERENCES

AWASTHI, M. 2012 High Reynolds number turbulent boundary layer flow over small forward facing steps. MS thesis, Virginia Polytechnic Institute and State University. http://scholar.lib.vt.edu/theses/available/etd-06292012-120614/.

BATCHELOR, G. K. 1953 *The Theory of Homogeneous Turbulence*. Cambridge University Press.

BEARMAN, P. W. 1971 Corrections for the effect of ambient temperature drift on hot-wire measurements in incompressible flow. *DISA Inform.* **11**, 25–30.

BLAKE, W. 1970 Turbulent boundary layer wall-pressure fluctuations on smooth and rough walls. *J. Fluid Mech.* **44**, 637–660.

BRADSHAW, P. 1967 Inactive motion and pressure fluctuations in turbulent boundary layers. *J. Fluid Mech.* **30**, 241–258.

CAMUSSI, R., FELLI, M., PEREIRA, F., ALOISIO, G. & DI MARCO, A. 2008 Statistical properties of wall pressure fluctuations over a forward-facing step. *Phys. Fluids* **20** (7), 075113.

CAMUSSI, R., GUJ, G. & RAGNI, A. 2006 Wall pressure fluctuations induced by turbulent boundary layers over surface discontinuities. *J. Sound Vib.* **294** (1–2), 177–204.

CASTRO, I. P. & EPIK, E. 1998 Boundary layer development after a separated region. *J. Fluid Mech.* **374**, 91–116.

CHERRY, N. J., HILLIER, R. & LATOUR, M. E. M. P. 1984 Unsteady measurements in a separated and reattaching flow. *J. Fluid Mech.* **144**, 13–46.

DEVENPORT, W. J., BURDISSO, R. A., BORGOLTZ, A., RAVETTA, P. A., BARONE, M. F., BROWN, K. A. & MORTON, M. A. 2013 The Kevlar-walled anechoic wind tunnel. *J. Sound Vib.* **332** (17), 3971–3991.

DEVENPORT, W. J., GRISSOM, D. L., ALEXANDER, W. N., SMITH, B. S. & GLEGG, S. A. L. 2011 Measurements of roughness noise. *J. Sound Vib.* **330**, 4250–4273.

EATON, J. K. & JOHNSTON, J. P. 1981 A review of research on subsonic turbulent flow reattachment. *AIAA J.* **19** (9), 1093–1100.

EFIMSTOV, B. M., GOLUBEV, A. Y., RIZZI, S. A., ANDERSSON, A. O., RACKL, R. G. & ANDRIANOV, E. V. 2002 Influence of small steps on wall pressure fluctuation spectral measured on a TU144LL flying laboratory. *AIAA Paper* 2002-2605.

https://doi.org/10.1017/jfm.2014.405 Published online by Cambridge University Press

EFIMTSOV, B. M., KOZLOV, N. M., KRAVCHENKO, S. V. & ANDERSSON, A. O. 1999 Wall pressure fluctuation spectra at small forward facing steps. *AIAA Paper* 99-1964.

FARABEE, T. M. & CASARELLA, M. J. 1986 Measurements of fluctuating wall pressure for separated/reattached boundary layer flows. *ASME J. Vib. Acoust. Stress Reliab. Des.* **108**, 301–307.

FIORENTINI, E., FELLI, M., PEREIRA, F., CAMUSSI, R. & DI MARCO, A. 2007 Wall pressure fluctuations over a forward-facing step. *AIAA Paper* 2007-8411.

GEORGE, W. K., BEUTHER, P. D. & ARNDT, R. E. A. 1984 Pressure spectra in turbulent free shear flows. *J. Fluid Mech.* **148**, 155–191.

GOODY, M. 2004 Empirical spectral model of surface pressure fluctuations. *AIAA J.* **42** (9), 1788–1794.

HILLIER, R. & CHERRY, N. J. 1981 The effects of stream turbulence on separation bubbles. *J. Wind Engng Ind. Aerodyn.* **8** (1–2), 49–58.

HORNE, P. 1990 Physical and computational investigation of the wall pressure fluctuations in a channel flow. *NRL Memorandum Report* 6628, Naval Research Laboratory.

JI, M. & WANG, M. 2010 Sound generation by turbulent boundary layer flow over small steps. *J. Fluid Mech.* **654**, 161–193.

JI, M. & WANG, M. 2012 Surface pressure fluctuations on steps immersed in turbulent boundary layers. *J. Fluid Mech.* **712**, 471–504.

KIYA, M. & SASAKI, K. 1983 Structure of a turbulent separation bubble. *J. Fluid Mech.* **137**, 83–113.

KIYA, M. & SASAKI, K. 1985 Structure of large-scale vortices and unsteady reverse flow in the reattaching zone of a turbulent separation bubble. *J. Fluid Mech.* **154**, 463–491.

LARGEAU, J. F. & MORINIERE, V. 2007 Wall pressure fluctuations and topology in separated flows over a forward-facing step. *Exp. Fluids* **42** (1), 21–40.

LECLERCQ, D. J. J., JACOB, M. C., LOUISOT, A. & TALOTTE, C. 2001 Forward–backward facing step pair: aerodynamic flow, wall pressure and acoustic characterization. *AIAA Paper* 2001-2249.

LEE, L. & SUNG, H. J. 2001 Characteristics of wall pressure fluctuations in separated and reattaching flows over a backward-facing step: part 1. Time-mean statistics and cross-spectral analyses. *Exp. Fluids* **30**, 262–272.

LEE, I. & SUNG, H. J. 2002 Multiple-arrayed pressure measurement for investigation of the unsteady flow structure of a reattaching shear layer. *J. Fluid Mech.* **463**, 377–402.

MCGRATH, B. E. & SIMPSON, R. L. 1987 Some features of surface pressure fluctuations in turbulent boundary layers with zero and favorable pressure gradients. *NASA* CR-4051.

PANTON, R. & LINEBARGER, J. 1974 Wall pressure spectra calculations for equilibrium boundary layers. *J. Fluid Mech.* **65** (2), 261–287.

SHERRY, M. J., JOCONO, D. L., SHERIDAN, J., MATHIS, R. & MARUSIC, I. 2009 Flow separation characterization of a forward facing step immersed in a turbulent boundary layer. In *Sixth Symposium on Turbulence and Shear Flow Phenomena, Seoul, South Korea, 22–24 June*.

STEINWOLF, A. & RIZZI, S. A. 2006 Non-Gaussian analysis of turbulent boundary layer fluctuating pressure on aircraft skin panels. *J. Aircraft* **43** (6), 1662–1675.

TACHIE, M. F., BALACHANDAR, R. & BERGSTROM, D. J. 2001 Open channel boundary layer relaxation behind a forward facing step at low Reynolds numbers. *Trans. ASME J. Fluids Engng* **123** (3), 539–544.

WITTMER, K. S., DEVENPORT, W. J. & ZSOLDOS, J. S. 1998 A four sensor hot wire probe system for three component velocity measurements. *Exp. Fluids* **24**, 416–423; see also 27(4), U1.

https://doi.org/10.1017/jfm.2014.405 Published online by Cambridge University Press